



## OPEN ACCESS

## EDITED BY

Farruh Atamurotov,  
Inha University in Tashkent, Uzbekistan

## REVIEWED BY

Hernando Quevedo,  
National Autonomous University of  
Mexico, Mexico  
Jan Schee,  
Silesian University in Opava, Czechia

## \*CORRESPONDENCE

Abhishek Chowdhuri,  
✉ chowdhuri\_abhishek@iitgn.ac.in  
Saptaswa Ghosh,  
✉ saptaswaghosh@iitgn.ac.in  
Arpan Bhattacharyya,  
✉ abhattacharyya@iitgn.ac.in

## SPECIALTY SECTION

This article was submitted to High-Energy and Astroparticle Physics, a section of the journal *Frontiers in Physics*

RECEIVED 01 December 2022

ACCEPTED 20 February 2023

PUBLISHED 21 March 2023

## CITATION

Chowdhuri A, Ghosh S and Bhattacharyya A (2023), A review on analytical studies in gravitational lensing. *Front. Phys.* 11:1113909. doi: 10.3389/fphy.2023.1113909

## COPYRIGHT

© 2023 Chowdhuri, Ghosh and Bhattacharyya. This is an open-access article distributed under the terms of the [Creative Commons Attribution License \(CC BY\)](https://creativecommons.org/licenses/by/4.0/). The use, distribution or reproduction in other forums is permitted, provided the original author(s) and the copyright owner(s) are credited and that the original publication in this journal is cited, in accordance with accepted academic practice. No use, distribution or reproduction is permitted which does not comply with these terms.

# A review on analytical studies in gravitational lensing

Abhishek Chowdhuri\*, Saptaswa Ghosh\* and Arpan Bhattacharyya\*

Indian Institute of Technology Gandhinagar, Gandhinagar, India

In this study, we review some current studies on gravitational lensing for black holes, mainly in the context of general relativity. We mainly focus on the analytical studies related to lensing with references to observational results. We start with reviewing lensing in spherically symmetric Schwarzschild spacetime, showing how to calculate deflection angles before moving to the rotating counterpart, the Kerr metric. Furthermore, we extend our studies for a particular class of newly proposed solutions called black-bounce spacetimes and discuss throughout the review how to explore lensing in these spacetimes and how the various parameters can be constrained using available astrophysical and cosmological data.

## KEYWORDS

gravitational lensing, strong lensing, Einstein ring, black holes, deflection angle

## 1 Introduction

The importance of gravitational lensing began with Eddington's observation of the light deflection of the Sun [1]. The experiment proved to be one of the major milestones in favor of Einstein's theory of general relativity [2]. The theory has proved itself to be the most successful theory of classical gravity. However, GR has some hiccups in the form of singularities, not being able to understand the quantum theory of it, along with the ubiquitous nature of dark matter and dark energy, forcing us to conclude that maybe there is more to the story. Following this line of thought, efforts have been made to introduce modifications to the Einstein–Hilbert Lagrangian [3–14]. However, taking in a cue from Eddington, gravitational lensing still remains one of the most indispensable tools to check and put constraints on our theory parameters.

The theory behind gravitational lensing started when O. Lodge asked a simple question in [15] on the behavior of light in a gravitational field. Interestingly, he concluded that, unlike a convex lens, the gravitational field does not focus light rays into a focal point. However, a logarithmically shaped concave lens can indeed mimic the effect of a spherically symmetric gravitational field onto the light. Inspired by such insights, O. Chwolson came up with the possibility of observing ring-like images in cases of axial symmetry. Nowadays, these ring-like images are called Einstein rings [16, 17]. Remarkably, such images were indeed observed by J. Hewitt et al. using the Very Large Array, a collection of radio telescopes in the United States. The radio source was MG1131 + 0456, and it was found when a background (radio) Galaxy is distorted into an almost closed ring [18–20]. Later, such rings were also found in the infrared and even in the optical spectrum [21] and more recently by the James Webb Telescope [22]. Typically, the diameter ranges between a few arcseconds or less.

The discovery of quasars and such rings lead to a rapid change in the field of gravitational lensing. We are now well aware of lensing techniques such as weak lensing, where the small deformations of many background galaxies are statistically evaluated for determining the

(dark) matter in a foreground Galaxy cluster, and microlensing, where the light curve of a star is registered that moves transversely to the line of sight behind a (dark and compact) mass. For a thorough exposition of gravitational lensing, including an overview of all pre-1992 observations, the reader may consult the monograph [23]. More up-to-date information can be found in [24].

In all the lensing observations mentioned previously, the bending angles are so small that a weak-field approximation for the gravitational field is applicable. A much simpler quasi-Newtonian formalism has been used. This approximation centers around a so-called lens map or lens equation, which is very intuitive. This lens map of the weak-field formalism has proven extremely useful for evaluating the aforementioned lensing phenomena. It is discussed in detail, for example, in [23]. Additional material can be found, for example, in the Living Review by Wambsganss [25], which is completely based on this approximation formalism. However, there are astrophysical scenarios where the bending angles are not small. In such cases, the weak lensing theory is not valid anymore. The objective of this review is to give an overview of the various analytical techniques used to study strong lensing and to give some insights into the relation of lensing parameters to the gravity theory itself.

This expectation is nurtured mainly by the increasing evidence of a black hole at the center of our Galaxy. Black holes arise as solutions of GR and play an important role in testing various aspects of it. Recent observations coming from the “Event Horizon Telescope” (EHT) [26–38] collaboration and LIGO, Virgo, and KAGRA collaboration [39–44] have provided us with enough observational evidence that ensures the existence of supermassive black holes. Furthermore, these observations provide a unique opportunity to test various aspects of strong gravity [45–55]. This necessitates us to go beyond weak-field approximation and consider lensing by the strong gravitational field, thereby motivating us to consider the strong-field limit of the bending angle. It provides important information about the intrinsic parameters such as spin, mass, and charge of the black holes and the parameters of the underlying gravity theory. Hence, its observational implications have been investigated in recent times<sup>1</sup>. An analytical description of the deflection angle for the spherically symmetric black hole in the strong gravitational field has been proposed in [76]. This was further based on [77, 78]. Later, it was extended for rotating black holes in [79]. A lens equation has been derived in [77], which has been further generalized in [80] where the underlying black hole serves as a lens. Numerous investigation of Einstein rings [81] and strong gravitational lensing based on the work has been made for various black hole spacetimes and compact objects<sup>2</sup>.

It should be noted that in this review, we will be focusing on the analytical computation of the deflection angle of light rays using null geodesic equations. However, there are other methods of calculating the deflection angle analytically, for instance, the *material medium approach*. In this approach, one maps the problem effectively to a problem of light propagation through a medium with a particular refractive index determined by the strength of the gravitational field

of the original spacetime for which one wants to calculate the deflection angle. For more details, interested readers are referred to [121–133] and citations of these references.

Furthermore, in recent times, several static metrics known as the *black-bounce metric* have been proposed in [134–137]. What makes this spacetime interesting is that they have an extra parameter which regularizes the central singularity, unlike the usual black hole spacetime. The black-bounce spacetime interpolates between a black hole and (traversable) wormhole metric depending on the choice of underlying regularization parameters. When the solution does not admit any horizon, it corresponds to a wormhole solution. Recently, the gravitational lensing in the strong deflection limit for these black-bounce spacetimes has been studied [120, 138–141]. From the lensing perspective, this kind of spacetime provides us with extra tunable parameters; hence, it is interesting to investigate the effect of this extra parameter from the theoretical and observational points of view. In this review, besides discussing some analytical results about the computation of the strong deflection angle in the background of Schwarzschild and Kerr–Newman black holes, we also discuss the effect of this black-bounce regularization parameter on the computation of the deflection angle and, finally, on the radius of the Einstein ring.

This article is organized as follows. In Section 2, we first review the deflection angle, the angular radius of Einstein rings, and Shapiro time delay for a Schwarzschild spacetime. In Section 3, we review a general formalism of computation of the equatorial deflection angle for Kerr–Newman spacetime. Then, in Section 4, we discuss the computation of the deflection angle for the black-bounce metric. We also review the computation of the Einstein ring radius of this case and comment on its dependence on charge and regularization parameters and its observational implications. Finally, we give concluding remarks in Section 5. Some necessary details are given in Appendix A. Also, we have set the value of the speed of light  $c$  and Newton’s gravitational constant  $G$  to unity.

## 2 Lensing for the spherically symmetric Schwarzschild black hole

In this section, we start by reviewing gravitational lensing in the simplest setup, that is, for the Schwarzschild solution. The metric reads

$$ds^2 = -\left(1 - \frac{2M}{r}\right)dt^2 + \frac{dr^2}{1 - \frac{2M}{r}} + r^2(d\theta^2 + \sin^2\theta d\phi^2). \quad (2.1)$$

The Lagrangian for the particle  $\bar{L} = \frac{1}{2}g_{\mu\nu}(x)\dot{x}^\mu\dot{x}^\nu$  reads

$$\bar{L} = \frac{1}{2}g_{\mu\nu}(x)\dot{x}^\mu\dot{x}^\nu = \frac{1}{2}\left[-\left(1 - \frac{2M}{r}\right)\dot{t}^2 + \frac{\dot{r}^2}{1 - \frac{2M}{r}} + r^2\dot{\phi}^2\right]. \quad (2.2)$$

We are only considering geodesics on the equatorial plane, where  $\theta = \frac{\pi}{2}$ . Hence,  $\sin\theta = 1$  along these geodesics and since  $\theta$  is fixed, every  $\dot{\theta}$  component is 0. Owing to the symmetry of the solution, we have two constants of motion which we can read off from the Euler–Lagrange equations. The  $t$ -component of the equation of motion gives

$$\left(1 - \frac{2M}{r}\right)\dot{t} = E = \text{constant}, \quad (2.3)$$

<sup>1</sup> This list is by no means exhaustive. Interested readers are referred to this review [24] and citations there for more details.

<sup>2</sup> Again, this list is by no means exhaustive. Interested readers are referred to the references and citations of these papers.

while the  $\phi$  component gives

$$r^2 \dot{\phi} = L = \text{constant}. \tag{2.4}$$

In this article, we will mainly focus on the lensing of light rays<sup>3</sup>. Hence, we will be considering the light-like trajectories with the null ray condition defined as follows:

$$g_{\mu\nu} \dot{x}^\mu \dot{x}^\nu = 0. \tag{2.5}$$

Hence,

$$-\left(1 - \frac{2M}{r}\right) \dot{t}^2 + \frac{\dot{r}^2}{1 - \frac{2M}{r}} + r^2 \dot{\phi}^2 = 0. \tag{2.6}$$

Then, we write the  $r$  component of the equation of motion in terms of the  $\phi$  component. To obtain that, we divide (2.3) by (2.4) and also define the impact parameter as

$$\lambda = \frac{L}{E}. \tag{2.7}$$

Then, we obtain

$$\frac{dt}{d\phi} = \frac{\dot{t}}{\dot{\phi}} = \frac{r^2}{\lambda \left(1 - \frac{2M}{r}\right)}. \tag{2.8}$$

Then, using (2.6), we obtain

$$\left(\frac{dr}{d\phi}\right)^2 = \frac{r^4}{\lambda^2} - r^2 \left(1 - \frac{2M}{r}\right). \tag{2.9}$$

Eqs 2.8, 2.9 provide all the necessary information regarding the behavior of light-like geodesics. Considering Eq. 2.9 and taking the  $\phi$  derivative of this equation, we obtain

$$2 \frac{dr}{d\phi} \frac{d^2 r}{d\phi^2} = \left(\frac{4r^3}{\lambda^2} - 2r + 2M\right) \frac{dr}{d\phi}. \tag{2.10}$$

For circular light-like geodesics, we must have  $\frac{dr}{d\phi} = 0$  and  $\frac{d^2 r}{d\phi^2} = 0$  which gives

$$\begin{aligned} \frac{r^4}{\lambda^2} - r^2 \left(1 - \frac{2M}{r}\right) &= 0, \\ \frac{4r^3}{\lambda^2} - 2r + 2M &= 0. \end{aligned} \tag{2.11}$$

By eliminating  $\lambda$  from the aforementioned equations, we obtain  $r = 3M$ . We have, thus, shown that there is a circular light-like geodesic (or photon ring)  $r = 3M$ . As we can choose any plane through the origin as our equatorial plane, there is actually a photon ring at this radius in the sense that every great circle on this sphere is a light-like geodesic. However, the photon rings at  $r = 3M$  are unstable in the following sense: a light-like geodesic with an initial condition that deviates slightly from that of a photon ring at  $r = 3M$  will spiral away from  $r = 3M$  and either go to infinity or to the horizon.

Now that we have understood how the null geodesics behave in this geometry, it is time to focus on deriving actual observable quantities that one can measure. For this, we go on to study them in

the upcoming sections one by one starting with calculating deflection angles.

## 2.1 Formula for the deflection angle

First, we set up the problem that we want to address. We consider a light ray that comes in from infinity and then goes through a minimum radius value at  $r = r_{min}$  and then escapes back to infinity. Due to the geometry of spacetime around the central black hole, which for us is a Schwarzschild one, there will be a deflection. This deflection is simply because the rectilinear propagation of light will not be observed in this non-trivial geometry. The deflection angle measures the degree of this deviation from rectilinear propagation. In the following discussion, we will express this in terms of  $r_{min}$  and the mass of the central object.

We start out with (2.7) and determine the ratio  $\frac{1}{\lambda^2}$  at  $r = r_{min}$ . This gives

$$\frac{1}{\lambda^2} = \frac{1}{r_{min}^2} - \frac{2M}{r_{min}^3}. \tag{2.12}$$

Hence, replacing this in (2.7), we obtain

$$d\phi = \frac{\pm dr}{\sqrt{\left(\frac{1}{r_{min}^2} - \frac{2M}{r_{min}^3}\right)r^4 - r^2 + 2Mr}} \tag{2.13}$$

which, on integrating over the coordinates of the light ray, leads to

$$\begin{aligned} \pi + \hat{\alpha} &= 2 \int_{r_{min}}^{\infty} \frac{r_{min} dr}{\sqrt{\left(1 - \frac{2M}{r_{min}}\right)r^4 - r^2 + 2Mr_{min}r}} \\ &= 2 \int_{r_{min}}^{\infty} \frac{r_{min} dr}{\sqrt{r^2(r^2 - r_{min}^2) - \frac{2M}{r_{min}}(r^3 - r_{min}^3)}} \\ &= 2 \int_{r_{min}}^{\infty} \frac{r_{min} dr}{\sqrt{1 - \frac{2M}{r_{min}} \frac{(r^3 - r_{min}^3)}{r(r^2 - r_{min}^2)}} r \sqrt{r^2 - r_{min}^2}} \\ &= 2 \int_{r_{min}}^{\infty} \left\{ 1 + \frac{1}{2} \frac{2M}{r_{min}} \frac{(r^3 - r_{min}^3)}{r(r^2 - r_{min}^2)} + \mathcal{O}\left(\frac{2M}{r_{min}}\right)^2 \right\} \frac{r_{min} dr}{r \sqrt{r^2 - r_{min}^2}} \\ &= 2 \int_{r_{min}}^{\infty} \frac{r_{min} dr}{r \sqrt{r^2 - r_{min}^2}} + \frac{2M}{r_{min}} \int_{r_{min}}^{\infty} \frac{(r^3 - r_{min}^3) r_{min} dr}{r^2 (r^2 - r_{min}^2)^{3/2}} + \mathcal{O}\left(\frac{2M}{r_{min}}\right)^2 \\ &= \pi + \frac{4M}{r_{min}} + \mathcal{O}\left(\frac{2M}{r_{min}}\right)^2. \end{aligned} \tag{2.14}$$

By neglecting higher-order terms, we obtain

$$\hat{\alpha} = \frac{4M}{r_{min}}. \tag{2.15}$$

Now, we will look at a point or two about this derivation:

- From the derivation, it is clear that the integrand has a singularity at the lower bound  $r = r_{min}$ . A more detailed analysis shows that the integral is finite for all values of  $r = r_{min}$  that are bigger than  $\frac{3}{2}r_s$ , where  $r_s = 2M$ . If we consider a sequence of light rays with  $r = r_{min}$  approaching  $\frac{3}{2}r_s$  from earlier, the deflection angle  $\delta$  becomes bigger and bigger, which means that the light rays make more and more turns around the center. In the limit  $r_{min} \rightarrow \frac{3}{2}r_s$ , the integral goes to infinity, and the limiting light ray spirals

<sup>3</sup> For deflection of the massive particle, one needs to consider time-like trajectories given by  $g_{\mu\nu} \dot{x}^\mu \dot{x}^\nu = -1$ .

asymptotically toward a circle at  $r = \frac{3}{2} r_s$ . If an unstable photon ring is approached, the deflection angle goes to infinity, and the singularity is logarithmic.

- The second point comes during the discussion on taking the Taylor series expansion in  $\frac{r_s}{r_{min}}$  in the fourth step. The asymptotic behavior of light rays for  $r_{min}$  approaching  $\frac{3}{2}r_s$  is relevant only for black holes and for ultracompact stars. For an ordinary star, like our Sun,  $r_{min}$  takes a value much bigger than  $r_s$ . It is under this consideration that we take a Taylor series expansion in  $\frac{r_s}{r_{min}}$ .

## 2.2 Shapiro time

Combining Eqs. 2.8 and 2.9 allows us to calculate the time taken by the light ray in this particular geometry. Here, we consider a light ray that starts at a radius  $r_L$ , passes through a minimum of radius  $r_{min}$ , and terminates at a radius  $r_O$ . From Eqs. 2.8 and 2.9, we obtain

$$\begin{aligned} \left(\frac{dr}{dt}\right)^2 &= \left(\frac{dr}{d\phi}\right)^2 \left(\frac{d\phi}{dt}\right)^2 = \left\{ \frac{r^4}{\lambda^2} - r^2 \left(1 - \frac{2M}{r}\right) \right\} \frac{\left(1 - \frac{2M}{r}\right)^2}{\lambda^2 r^4} \\ &= \left\{ \frac{r^3}{\lambda^2} - r \left(1 - \frac{2M}{r}\right) \right\} \frac{(r - 2M)^2}{\lambda^2 r^5}. \end{aligned} \tag{2.16}$$

At  $r = r_{min}$ , (2.16) reads

$$\frac{r_{min}^4}{\lambda^2} - r_{min}^2 \left(1 - \frac{2M}{r_{min}}\right) = 0 \Rightarrow \frac{1}{\lambda^2} = \frac{r_{min} - 2M}{r_{min}^3}. \tag{2.17}$$

Finally, (2.16) becomes

$$\left(\frac{dr}{dt}\right)^2 = \left\{ \frac{(r_{min} - 2M)r^3}{r_{min}^3} - r \left(1 - \frac{2M}{r}\right) \right\} \frac{(r - 2M)r_{min}^3}{(r_{min} - 2M)r^5}, \tag{2.18}$$

which gives

$$dt = \frac{\pm \sqrt{r_{min} - 2M} r^{5/2} dr}{(r - 2M)r_{min}^{3/2} \sqrt{\frac{(r_{min} - 2M)r^3}{r_{min}^3} - r \left(1 - \frac{2M}{r}\right)}}. \tag{2.19}$$

By integrating, we obtain the travel time for the light ray,

$$\Delta t = \left( - \int_{r_L}^{r_{min}} + \int_{r_{min}}^{r_O} \right) \frac{\sqrt{r_{min} - 2M} r^{5/2} dr}{(r - 2M)r_{min}^{3/2} \sqrt{\frac{(r_{min} - 2M)r^3}{r_{min}^3} - r \left(1 - \frac{2M}{r}\right)}} \tag{2.20}$$

where the signs on the right-hand side had to be chosen in such a way that the time coordinate is always increasing along the light ray. One can perform this integral exactly in terms of an elliptic integral. However, when  $r_{min} \gg r_s$ , we can make a Taylor approximation, in exactly the same way as we did it for the deflection formula, and obtain

$$\begin{aligned} \Delta t &= \left( \int_{r_{min}}^{r_L} + \int_{r_{min}}^{r_O} \right) \frac{r dr}{\sqrt{r^2 - r_{min}^2}} + 2M \left( \int_{r_{min}}^{r_L} + \int_{r_{min}}^{r_O} \right) \frac{dr}{\sqrt{r^2 - r_{min}^2}} \\ &+ \frac{2Mr_{min}}{2} \left( \int_{r_{min}}^{r_L} + \int_{r_{min}}^{r_O} \right) \frac{dr}{\sqrt{r - r_{min}} (r + r_{min})^{3/2}} + \dots \end{aligned} \tag{2.21}$$

The zeroth-order term is, of course, the Euclidean travel time for a light ray with speed  $c$  along a straight line. The deviation of the

general-relativistic calculation from this zeroth-order term is known as the Shapiro time delay [142].

I. Shapiro suggested using this effect as the fourth test of general relativity (after perihelion precession, light deflection, and gravitational redshift). In the first experiment, a strong radio signal was sent to Venus when it was in opposition to Earth, and the time was measured until the signal arrived back on Earth after being reflected in Venus's atmosphere. Later experiments were performed with transponders on spacecraft, which sent the signal back with increased intensity. The best measurement to date was performed with the Cassini spacecraft in 2002. The general-relativistic time delay was verified to be within an accuracy of 0.001% [142].

## 2.3 Angular radius of Einstein rings

An Einstein ring can be observed when the light source and observer are perfectly aligned (directly opposite to each other). We want to determine the angular radius  $\theta_E$  of the Einstein ring in dependence on the radius coordinate  $r_L$  of the light source, the radius coordinate  $r_O$  of the observer, and the Schwarzschild radius ( $= 2M$ ). We use the formula

$$d\phi = \frac{\pm dr}{\sqrt{\frac{(r_{min} - \frac{2M}{c^2})r^4}{r_{min}^3} - r^2 + 2Mr}}. \tag{2.22}$$

Integrating over the light ray gives

$$\pi = \left( \int_{r_{min}}^{r_L} + \int_{r_{min}}^{r_O} \right) \frac{dr}{\sqrt{\frac{(r_{min} - \frac{2M}{c^2})r^4}{r_{min}^3} - r^2 + 2Mr}} \tag{2.23}$$

The integration gives

$$r_{min} = f(r_L, r_O, 2M). \tag{2.24}$$

With  $r_{min}$  determined, the angular radius of the Einstein ring can be obtained by

$$\tan \theta_E = \frac{r d\phi}{\left(1 - \frac{2M}{r}\right)^{-1/2} dr} \Big|_{r=r_O}. \tag{2.25}$$

## 3 Lensing for the Kerr–Newman black hole

In Section 2, we discussed the gravitational lensing in Schwarzschild spacetime. We expand the integrand around the turning point to obtain a simplified result, but in principle, we can calculate the exact deflection angle. In this section, first and foremost, we will generalize the result of lensing for rotating spacetime. We will calculate the deflection angle for the light rays in Kerr–Newman spacetime which is an axisymmetric spacetime. One can reproduce the result for the Kerr and Schwarzschild case as special limits. We will also discuss the strong deflection angle's analytical form. We will closely follow the notation in [120].

In Boyer–Lindquist, the line element is given by

$$ds^2 = -\frac{\Delta}{\Sigma}(dt - a \sin^2 \theta d\phi)^2 + \Sigma \left( \frac{dr^2}{\Delta} + d\theta^2 \right) + \frac{\sin^2 \theta}{\Sigma} (a dt - (r^2 + a^2) d\phi)^2, \tag{3.1}$$

where

$$\Sigma = r^2 + a^2 \cos^2 \theta, \Delta(r) = \Delta(r) = (r^2 + a^2) - 2mr + Q^2. \tag{3.2}$$

In (3.3) and (3.2),  $m \geq 0$ ,  $Q$ , and  $a$  are, respectively, the ADM mass, charge, and angular momentum of the black hole. As we know, the particle Lagrangian, specifically for the photons, is given by (2.2), with  $\dot{x}^\mu = \frac{dx^\mu}{d\tilde{\lambda}}$  for some convenient parameter  $\tilde{\lambda}$ . The metric coefficients are independent of  $t$  and  $\phi$ , implying that we will have two conserved quantities along the photon trajectory: energy  $E$  and angular momentum  $L$ . Using the constants of motion and the null ray condition in (2.5), the null geodesic equations can be written as follows:

$$\begin{aligned} \rho^4 \dot{r}^2 &= ((r^2 + a^2)E - aL)^2 - \Delta(r) ((L - aE)^2 + \bar{K}) := R^2(r), \\ \Sigma \dot{\phi} &= -\left( aE - \frac{L}{\sin^2 \theta} \right) + \frac{a[E(r^2 + a^2) - aL]}{\Delta}, \\ \Sigma \dot{t} &= -a(aE \sin^2 \theta - L) + \frac{(r^2 + a^2)[E(r^2 + a^2) - aL]}{\Delta}, \\ \rho^4 \dot{\theta}^2 &= \bar{K} + \cos^2 \theta \left( a^2 E^2 - \frac{L^2}{\sin^2 \theta} \right) := \Theta(\theta)^2 \end{aligned} \tag{3.3}$$

where the Carter constant, which results from the separability of the Hamilton–Jacobi equation, is  $\bar{K}$ . For our purpose, we will look upon into the equatorial case only, that is,  $\theta = \frac{\pi}{2}, \dot{\theta} = 0$  which automatically implies  $\bar{K} = 0$ , and then will investigate the non-equatorial case also. We can use the geodesic equations to calculate the equatorial deflection angle. Rather in the next section, we will provide the deflection angle calculations and reproduce the result for Kerr by taking the limit  $Q = 0$ .

### 3.1 Deflection angle for Kerr–Newman spacetime

From (3.3), we can write the radial geodesic equations as follows:

$$\frac{\dot{r}^2}{L^2} + V(r) = \frac{1}{\lambda^2}, \tag{3.4}$$

with the effective potential

$$V(r) = \frac{1}{r^2} \left[ 1 - \frac{a^2}{\lambda^2} + \left( 1 - \frac{a}{\lambda} \right)^2 \left( -\frac{2m}{r} + \frac{Q^2}{r^2} \right) \right], \tag{3.5}$$

and  $\lambda$  is the impact parameter defined in (2.7).

Now, we think of light rays that originate at infinity, pass through the black hole, and then, return to infinity to reach the observer. The closest approach to the black hole,  $r_0$ , will be the radial turning point for these light rays, determined by

$$\left( \frac{\dot{r}^2}{L^2} \right) \Big|_{r=r_0} = \frac{1}{\lambda^2} - V(r_0) = 0. \tag{3.6}$$

From (3.6), we obtain

$$r_0^4 - \lambda^2 \left( 1 - \frac{a^2}{\lambda^2} \right) r_0^2 + 2m\lambda^2 \left( 1 - \frac{a}{\lambda} \right)^2 r_0 = Q^2 \lambda^2 \left( 1 - \frac{a}{\lambda} \right)^2. \tag{3.7}$$

Solving (3.7), we obtain

$$r_0(\lambda) = \frac{\lambda}{\sqrt{6}} \sqrt{1 - \omega^2} \left[ \sqrt{1 + \hat{\gamma}} + \sqrt{2 - \hat{\gamma} - \frac{3\sqrt{6} m (1 - \omega)^2}{\lambda (1 - \omega^2)^{3/2} \sqrt{1 + \hat{\gamma}}}} \right], \tag{3.8}$$

where  $\omega, \chi, \rho, \hat{\gamma}$  are given by

$$\begin{aligned} \omega &= \frac{a}{\lambda}, \rho = \frac{12Q^2}{\lambda^2 (1 + \omega)^2}, \hat{\gamma} = \sqrt{1 - \rho} \cos\left(\frac{2\chi}{3}\right), \\ \chi &= \arccos\left( \frac{3\sqrt{3} m (1 - \omega)^2}{\lambda (1 - \omega^2)^{3/2} (1 - \rho)^{3/4}} \sqrt{1 - \frac{\lambda^2 (1 + \omega)^3}{54 m^2 (1 - \omega)} [1 + 3\rho - (1 - \rho)^{3/2}]} \right). \end{aligned} \tag{3.9}$$

One can convince that the non-zero charge of the black holes gives a repulsive effect on the light rays, but the effect of spin attracts the light rays toward the black hole.

### 3.2 Photon sphere radius and critical impact parameter

In this subsection, we will define the photon sphere and the critical impact parameter which will be useful in the subsequent sections. The radius of the photon sphere is the value of  $r$  where the effective potential attains its maximum value.

$$\left. \frac{\partial V(r)}{\partial r} \right|_{r=r_c} = 0. \tag{3.10}$$

From (3.10), we can find out

$$r_c(\lambda_c) = \frac{3m\hat{\zeta}}{2} \left[ 1 + \sqrt{1 - \zeta} \right], \tag{3.11}$$

where

$$\hat{\zeta} = \left( \frac{1 - \frac{a}{\lambda_c}}{1 + \frac{a}{\lambda_c}} \right), \quad \zeta = \frac{8Q^2}{9m^2} \hat{\zeta}.$$

It should be noted that the turning point of the photon is  $r_0$  defined in (3.8) and attains its minimum value at  $r_c$  with the corresponding impact parameter  $\lambda_c$ . If for some  $\lambda$ ,  $r_0$  becomes less than  $r_c$ , then the photon will fall into the black hole.  $\lambda_c$  is called the critical impact parameter. Finally, substituting Eq. 3.8 into (3.11), we can write  $\lambda_c = \lambda_c(a, Q, l)$  and  $r_c = r_c(a, Q, l)$ .

### 3.3 An exact analytical computation of the deflection angle

In this subsection, we will compute the exact photon deflection angle near a Kerr–Newman black hole. To perform this, we can choose any polar plane, but to keep things simple, we choose the equatorial plane  $\theta = \frac{\pi}{2}$  and  $\dot{\theta} = 0$ . Furthermore, to investigate the observational signature, we need to employ the strong deflection limit. To perform this, we have to evaluate the deflection angle in the mentioned plane and take the strong limit. We can rather perform the reverse procedure also; that is, from the beginning, we take the strong limit and then calculate the deflection angle at this limit. The second one is simpler to perform. We adopt this track while discussing the observational signature.

The analysis has been performed in [143, 144]. We review the analysis here. Before proceeding with the computation, we define the following coordinates:

$$u := \frac{1}{r}. \tag{3.12}$$

By combining the first two equations in (3.3), we obtain

$$\left(\frac{du}{d\phi}\right)^2 = \left(\frac{du}{dr} \frac{dr}{d\phi}\right)^2 = \frac{r^2}{r^6} \frac{\dot{r}^2}{\dot{\phi}^2} = (u^4) \frac{\dot{r}^2}{\dot{\phi}^2}. \tag{3.13}$$

Now, our goal is to rewrite  $\dot{r}$  and  $\dot{\phi}$  as a function of  $u$ . We have

$$\begin{aligned} \dot{r}^2 &= L^2 \left( \frac{1}{\lambda^2} - V(r) \right) \\ &= L^2 \left[ \frac{1}{\lambda^2} - \left[ \frac{1}{r^2} \left( 1 - \frac{a^2}{\lambda^2} + \left( 1 - \frac{a}{\lambda} \right)^2 \left( -\frac{2m}{r} + \frac{Q^2}{r^2} \right) \right) \right] \right] \\ &= L^2 \left[ \frac{1}{\lambda^2} - u^2 \left( 1 - \frac{a^2}{\lambda^2} \right) - Q^2 \left( 1 - \frac{a}{\lambda} \right)^2 u^4 + 2m \left( 1 - \frac{a}{\lambda} \right)^2 u^3 \right] := L^2 B(u). \end{aligned} \tag{3.14}$$

Combining Eqs 3.14 and 3.3 and using Eq. 3.13, we obtain

$$\left(\frac{du}{d\phi}\right)^2 = \left[ \frac{1 - 2mu + (a^2 + Q^2)u^2}{1 - (2mu - Q^2u^2)(1 - \frac{a}{\lambda})} \right]^2 B(u). \tag{3.15}$$

The photon deflection angle  $\hat{\alpha}$  can be calculated by integrating Eq. 3.15 over  $u$  from 0 to  $\frac{1}{r_0}$ , where  $r_0$  is the turning point, and then evaluating the resulting expression at the critical value  $r_c$  [79],

$$\hat{\alpha} = -\pi + 2 \int_0^{\frac{1}{r_0}} du \left[ \frac{1 - (2mu - Q^2u^2)(1 - \frac{a}{\lambda})}{1 - 2mu + (a^2 + Q^2)u^2} \right] \frac{1}{\sqrt{B(u)}}, \tag{3.16}$$

with  $\omega = \frac{a}{\lambda}$ . This integral can be computed exactly. We give the final result here. The details of the computation of this integral are given in Appendix A.

$$\begin{aligned} \hat{\alpha} &= -\pi + \frac{4}{(1-\omega)\sqrt{Q^2(u_4-u_2)(u_3-u_1)}} \\ &\times \left[ \frac{G_+ + K_{Q_+}u_1}{u_+ - u_1} [\Pi(n_+, k) - \Pi(n_+, \phi, k)] \right. \\ &+ \frac{G_- + K_{Q_-}u_1}{u_- - u_1} [\Pi(n_+, k) - \Pi(n_+, \phi, k)] \\ &- \frac{G_+ + K_{Q_+}u_4}{u_+ - u_4} \left[ \Pi(n_+, k) - \Pi[n_+, \phi, k] - F\left(\frac{\pi}{2}, k\right) + F(\phi, k) \right] \\ &\left. - \frac{G_- + K_{Q_-}u_4}{u_- - u_4} \left[ \Pi(n_-, k) - \Pi[n_-, \phi, k] - F\left(\frac{\pi}{2}, k\right) + F(\phi, k) \right] \right], \end{aligned} \tag{3.17}$$

where

$$\begin{aligned} u_1 &= \frac{X_1 - 2m - X_2}{4mr_0}, u_2 = \frac{1}{r_0}, u_3 = \frac{X_1 - 2m + X_2}{4mr_0}, u_4 = \frac{2m}{Q^2} - \frac{X_1}{2mr_0}, \\ n_{\pm} &= \frac{u_2 - u_1}{u_{\pm} - u_1} \left[ 1 + \frac{2mQ^2(1 - r_0u_{\pm})}{4m^2r_0 - Q^2(X_1 + 2m)} \right], \\ k^2 &= \frac{(X_2 + 6m - X_1)[8m^2r_0 - Q^2(X_2 - 2m + 3X_1)]}{4X_2[4m^2r_0 - Q^2(X_2 + 2m)]}, \\ \psi_0 &= \arcsin \sqrt{\frac{(X_2 + 2m - X_1)[4m^2r_0 - Q^2(X_2 + 2m)]}{(X_2 + 6m - X_1)(4m^2r_0 - Q^2X_1)}}, \\ G_{\pm} &= \frac{2m(1-\omega)\left(m + \sqrt{m^2 - (a^2 + Q^2)}\right) - (a^2 + Q^2)}{2(a^2 + Q^2)\sqrt{m^2 - (a^2 + Q^2)}}, \\ G_{\pm} &= \frac{(a^2 + Q^2) - 2m(1-\omega)\left(m - \sqrt{m^2 - (a^2 + Q^2)}\right)}{2(a^2 + Q^2)\sqrt{m^2 - (a^2 + Q^2)}}, \\ G_{Q_+} &= \frac{-Q^2(1-\omega)\left(m + \sqrt{m^2 - (a^2 + Q^2)}\right)}{2(a^2 + Q^2)\sqrt{m^2 - (a^2 + Q^2)}}, \\ G_{Q_-} &= \frac{Q^2(1-\omega)\left(m - \sqrt{m^2 - (a^2 + Q^2)}\right)}{2(a^2 + Q^2)\sqrt{m^2 - (a^2 + Q^2)}}. \end{aligned} \tag{3.18}$$

It should be noted that  $\Pi(n_+, \psi_0, k)$  and  $\Pi(n_+, k)$  are the incomplete and complete elliptic integral of the third kind, respectively. Also,  $F(\psi_0, k)$  and  $F(\frac{\pi}{2}, k)$  are the incomplete and complete elliptic integral of the first kind, respectively. Also,

$$X_1 = \frac{2m(Q^2 + 4mr_0)}{3Q^2} + \frac{8m^2r_0}{3Q^2} \sqrt{1 + \frac{Q^2}{2m^2} \left( \frac{m}{r_0} - \frac{3(1+\omega)}{2(1-\omega)} - \frac{Q^2}{r_0^2} \right)} \cos\left(\frac{\delta}{3} + \frac{2\pi}{3}\right), \tag{3.19}$$

where

$$\delta = \arccos\left(\frac{-8m^3r_0^3 - 3mQ^2r_0^2\left(2m - \frac{3r_0(1+\omega)}{(1-\omega)}\right) - 3Q^4r_0\left(5m - \frac{3r_0(1+\omega)}{(1-\omega)}\right) + 10Q^6}{\left[4m^2r_0^2 + Q^2r_0\left(2m - \frac{3r_0(1+\omega)}{(1-\omega)}\right) - 2Q^4\right]^{3/2}}\right), \tag{3.20}$$

and  $X_2$  can be obtained from the following equations after inserting  $X_1$  from (3.20).

$$\left[X_2^2 - (X_1^2 - 2m)^2\right] \left(\frac{1}{8mr_0^3} - \frac{Q^2X_1}{32m^3r_0^4}\right) = \frac{1}{\lambda^2(1-\omega)^2}. \tag{3.21}$$

So, the exact deflection angle can be derived as discussed. One can reproduce the results for the Schwarzschild black hole in the limit  $a \rightarrow 0$  and  $Q \rightarrow 0$  and the Kerr black hole in the limit  $a \rightarrow 0$ .

### 3.4 Strong deflection analysis for axisymmetric spacetime

In this section, we inspect the strong limit of the equatorial deflection angle ( $\theta = \frac{\pi}{2}$ ) of the light rays discussed in the previous section in order to gain further understanding of the deflection angle for our context and make touch with the feasible observational signature. The strong deflection limit of (4.14) is challenging to take directly. It will be simpler to perform the integration after taking the strong-field limit of the integrand of (4.4). We shall only take into account the photons having the turning point very close to the photon sphere's radius, as was previously specified.

The metric on the equatorial plane has the following structure:

$$ds^2 = -\bar{A}(r)dt^2 + \bar{B}(r)dr^2 + \bar{C}(r)d\phi^2 - \bar{D}(r)dt d\phi, \tag{3.22}$$

with

$$\begin{aligned} \bar{A}(r) &= \frac{(\Delta(r) - a^2)}{\Sigma}, \\ \bar{B}(r) &= \frac{\Sigma}{\Delta}, \\ \bar{C}(r) &= \frac{1}{\Sigma} \left[ (r^2 + a^2 + l^2)^2 - \Delta(r)a^2 \right], \\ \bar{D}(r) &= \frac{2}{\Sigma} \left[ (r^2 + a^2 + l^2)a - \Delta(r)a \right]. \end{aligned} \tag{3.23}$$

It should be noted that all metric components are evaluated in the equatorial plane. We have already seen that the spacetime admits two conserved quantities  $E$  and  $L$  due to the existing symmetries. To keep things simple, we set  $E = 1$ . As a result, the impact parameter is  $\lambda = L$ . Using the fact that at the distance of closest approach,  $r = r_0$  and  $\dot{r} = 0$ , we obtain the following results from (3.4):

$$\begin{aligned} L &= \frac{-\bar{D}_0 + \sqrt{4\bar{A}_0\bar{C}_0 + \bar{D}_0^2}}{2\bar{A}_0} \\ &= \frac{r_0 \left( r_0^2 \sqrt{a^2 - 2mr_0 + Q^2} + r_0^2 + a(Q^2 - 2mr_0) \right)}{Q^2r_0 + l^2(r_0 - 2m) + r_0^2(r_0 - 2m)}. \end{aligned} \tag{3.24}$$

The subscript “0” denotes that functions are evaluated at  $r = r_0$ . From the equation of motion of  $\phi$  [the second equation of (3.3)], we obtain

$$\phi(r_0) = 2 \int_{r_0}^{\infty} \frac{\sqrt{\bar{B}\bar{A}_0}(\bar{D} + 2L\bar{A})}{\sqrt{4\bar{A}\bar{C} + \bar{D}^2} \sqrt{\bar{C}\bar{A}_0 - \bar{A}\bar{C}_0 + L(\bar{A}\bar{D}_0 - \bar{D}\bar{A}_0)}} dr. \tag{3.25}$$

In the strong limit, we only consider the photons having closest approach  $r_c$  near to the radius of the photon sphere. To implement the limit, one can expand the deflection angle  $\hat{\alpha}$  around  $r_c$  or  $\lambda_c$  and perform the radial integral function. When the turning point  $r_0$  is greater than the radius of the photon sphere  $r_c$ , then we obtain a finite deflection angle; otherwise, the photon will be caught by the black hole and the deflection angle diverges. Following the method developed here [76, 79], it is easy to find out the nature of the divergence in the deflection angle when the photons are very close to the radius of the photon sphere  $r = r_c$ . One can define two variables  $y, z$  as

$$z_1 = \bar{A}(r), z_2 = \frac{z_1 - z_{1,0}}{1 - z_{1,0}}. \tag{3.26}$$

Now, the azimuthal angle defined in (3.25) can be expressed in terms of these two new variables,

$$\phi(r_0) = \int_0^1 \bar{R}(z_2, r_0) \bar{F}(z_2, r_0) dz_2, \tag{3.27}$$

where

$$\bar{R}(z_2, r_0) = \frac{2(1 - z_{1,0})}{A'} \frac{\sqrt{\bar{B}\bar{A}_0}(\bar{D} + 2L\bar{A})}{\sqrt{4\bar{A}\bar{C}^2 + \bar{C}\bar{D}^2}}, \tag{3.28}$$

$$\bar{F}(z_2, r_0) = \frac{1}{\sqrt{\frac{1}{C}(\bar{C}\bar{A}_0 - \bar{A}\bar{C}_0 + L(\bar{A}\bar{D}_0 - \bar{D}\bar{A}_0))}} = \frac{1}{\sqrt{H}} \tag{3.29}$$

$$\bar{H} = \frac{1}{C}(\bar{C}\bar{A}_0 - \bar{A}\bar{C}_0 + L(\bar{A}\bar{D}_0 - \bar{D}\bar{A}_0)). \tag{3.30}$$

The function  $\bar{R}(z, r_0)$  is regular for any  $z$  and  $r_0$  values, whereas the function  $\bar{F}(z, r_0)$  is divergent for  $z = 0$ , that is, at  $r = r_0$ . As a result, after extracting the divergent part, one can rewrite (3.25).

$$\phi(r_0) = \phi_{\bar{R}}(r_0) + \phi_{\bar{F}}(r_0), \tag{3.31}$$

where the divergent part can be written as follows:

$$\phi_{\bar{F}}(r_0) = \int_0^1 \bar{R}(z_2 = 0, r_c) \bar{F}_0(z_2, r_0) dz. \tag{3.32}$$

We know that the deflection angle should diverge at  $r_0 = r_c$ , indicating that the photon has been captured by the black hole. Next, we want to determine the nature of the divergence. Examining the denominator will allow us to determine the nature of the divergence (4.18). In order to achieve this, we Taylor expand the denominator of  $\bar{F}_0(r_0, z_2)$  (3.33) around  $z_2 = 0$ .

$$\bar{F}_0(z_2, r_0) \approx \frac{1}{\sqrt{\sigma_1(r_0)z + \sigma_2(r_0)z^2 + \mathcal{O}(z^3)}} \tag{3.33}$$

It is worth noting that if  $\sigma_1(r_0) = 0$  (this occurs when  $r_0$  coincides with the radius of the photon sphere [145]), then it is clear from (3.33) that the leading term is  $\frac{1}{z}$  in the small  $z$  limit. As a result, after integration, we obtain a logarithmic divergence, as shown in (3.42).

To find  $\sigma_1$  and  $\sigma_2$ , we first Taylor expand  $\bar{H}$ , which is defined in (4.21).

$$\bar{H}(z, r_0) = \bar{H}(0, r_0) + \left. \frac{\partial \bar{H}}{\partial z_2} \right|_{z_2=0} z_2 + \frac{1}{2!} \left. \frac{\partial^2 \bar{H}}{\partial z_2^2} \right|_{z_2=0} z_2^2 + \mathcal{O}(z_2^3), \text{ with } \bar{H}(0, r_0) = 0. \tag{3.34}$$

Therefore, using (4.20), we can identify  $\sigma_1$  and  $\sigma_2$  as

$$\sigma_1 := \left. \frac{\partial \bar{H}}{\partial z_2} \right|_{z_2=0} = \frac{1 - \bar{A}_0}{\bar{A}'_0 \bar{C}'_0} (\bar{A}_0 \bar{C}'_0 - \bar{A}'_0 \bar{C}_0 - L(\bar{A}_0 \bar{D}'_0 - \bar{A}'_0 \bar{D}_0)), \tag{3.35}$$

and

$$\sigma_2 := \frac{1}{2!} \left. \frac{\partial^2 \bar{H}}{\partial z_2^2} \right|_{z_2=0} = \frac{(1 - \bar{A}_0)^2}{2\bar{C}_0^2 \bar{A}_0'^3} \times [2\bar{C}_0 \bar{C}'_0 \bar{A}_0'^2 + (\bar{C}_0 \bar{C}''_0 - 2\bar{C}_0'^2) \bar{A}_0 \bar{A}'_0 - \bar{C}_0 \bar{C}'_0 \bar{A}_0 \bar{A}''_0 + L(\bar{A}_0 \bar{C}_0 (\bar{A}_0'' \bar{D}'_0 - \bar{A}'_0 \bar{D}''_0) + 2\bar{A}_0' \bar{C}'_0 (\bar{A}_0 \bar{D}'_0 - \bar{A}'_0 \bar{D}_0))]. \tag{3.36}$$

We can write the regular part as follows:

$$\phi_{\bar{R}}(r_0) = \int_0^1 \bar{G}(z_2, r_0) dz_2, \tag{3.37}$$

where  $\bar{G}(z_2, r_0) = \bar{R}(z_2, r_0) \bar{F}(z_2, r_0) - \bar{R}(z_2 = 0, r_c) \bar{F}_0(z_2, r_0)$ . The coefficient  $\sigma_1 = 0$ , in the strong deflection limit. This implies

$$\bar{A}_0 \bar{C}'_0 - \bar{A}'_0 \bar{C}_0 - L(\bar{A}_0 \bar{D}'_0 - \bar{A}'_0 \bar{D}_0) \Big|_{r_0=r_c} = 0. \tag{3.38}$$

From (3.38), we obtain

$$-2a(Q^2 - mr_c) \sqrt{a^2 - 2mr_c + Q^2 + r_c^2} + 2a^2(Q^2 - mr_c) + r_c^2(6m^2 - 5mr_c + r_c^2) + Q^2 r_c(3r_c - 7m) + 2Q^4 = 0 \tag{3.39}$$

It is simple to verify that the expression for the critical impact parameter  $\lambda_c$  found in (3.24) yields the identical expression for the radius of the photon sphere found in (3.11). The photon sphere is defined yet again by (4.25), according to this. Readers who are interested in learning more about the geometry of photon spheres and several complementary definitions of photon spheres are directed to [145].

For fixed values of  $Q, a$ , we can compute the radius of the photon sphere in Kerr–Newman spacetime. In the next section, we will discuss the more general case which is the Kerr–Newman black-bounce spacetime, and the solutions of the photon sphere equation will be discussed there in a more general setting.

We may now assess the divergent integral (4.23) with the help of the following equation:

$$\begin{aligned} \phi_{\bar{F}}(r_0 \approx r_c) &= \bar{R}(z_2 = 0, r_c) \int_0^1 \frac{1}{\sqrt{\sigma_1 z_2 + \sigma_2 z_2^2}} dz_2 \\ &= \bar{R}(z_2 = 0, r_0 \approx r_c) \frac{2}{\sqrt{\sigma_2}} \log \left( \frac{\sqrt{\sigma_2} + \sqrt{\sigma_2 + \sigma_1}}{\sqrt{\sigma_1}} \right). \end{aligned} \tag{3.40}$$

We are aware that the function  $\phi_{\bar{F}}(r_0)$  diverges when  $r_0 = r_c$ , or when the coefficient  $\sigma_1 = 0$ . In order to obtain the nature of

$\phi_{\bar{F}}(r_0 \approx r_c)$ , the idea is to expand the  $\sigma_1(r_0)$  around  $r_0 = r_c$  up to the first order and substitute it into (3.40).

$$\begin{aligned} \sigma_1(r_0) &= \left. \frac{\partial \sigma_1}{\partial r_0} \right|_{r_0=r_c} (r_0 - r_c) + \mathcal{O}(r_0 - r_c)^2, \\ \sigma_2(r_0) &= \sigma_2(r_c) + \left. \frac{\partial \sigma_2}{\partial r_0} \right|_{r_0=r_c} (r_0 - r_c) + \mathcal{O}(r_0 - r_c)^2. \end{aligned} \tag{3.41}$$

Substituting (3.41) into (3.40) and using condition (3.38), we obtain

$$\phi_{\bar{F}}(r_0 \approx r_c) = -\bar{a} \log\left(\frac{r_0}{r_c} - 1\right) + \bar{b} + \mathcal{O}(r_0 - r_c). \tag{3.42}$$

Alternatively, Eq. 3.42 can be written in terms of the impact parameter as [79]

$$\hat{\alpha}(\lambda) = -\bar{a} \log\left(\frac{\lambda}{\lambda_c} - 1\right) + \bar{b} + \mathcal{O}(\lambda - \lambda_c), \tag{3.43}$$

where the coefficients are

$$\bar{a} = \sqrt{\frac{2\bar{A}_c \bar{B}_c}{\bar{A}_c \bar{C}_c'' - \bar{A}_c'' \bar{C}_c + \lambda_c (\bar{A}_c'' \bar{D}_c - \bar{A}_c \bar{D}_c'')}}, \tag{3.44}$$

$$\bar{b} = -\pi + b_R + \bar{a} \log\left(\frac{4\sigma_{2c} \bar{C}_c}{\lambda_c \bar{A}_c (\bar{D}_c + 2\lambda_c \bar{A}_c)}\right), \tag{3.45}$$

$$\lambda_c = L_c. \tag{3.46}$$

In the next section, we will show how the deflection angle (3.43) varies with respect to the impact parameter. The black hole can be viewed as a lens, with its gravitational field curving the path of photons. Let  $\theta = \frac{\lambda}{D_{ol}}$  be the angular separation between the image and lens, and  $D_{ol}$  be the distance between the lens and the observer. The deflection angle (3.43) can then be expressed as follows:

$$\hat{\alpha}(\theta) = -\bar{a} \log\left(\frac{\theta D_{ol}}{\lambda_c} - 1\right) + \bar{b} + \mathcal{O}(\lambda - \lambda_c), \tag{3.47}$$

where  $b_R = \phi_{\bar{R}}(r_c) = \int_0^1 \bar{G}(z, r_c) dz$ .

In order to perform the integral function, we can expand  $\bar{R}(z, r_c)$  around  $z = 0$  and then put it in (4.23). Formally, we obtain the following expression:

$$b_R = \frac{1}{\sqrt{\sigma_2}} \int_0^1 \left( \frac{\bar{R}(z)}{z} - \frac{\bar{R}(0)}{z} \right) dz \Big|_{r_c} = \frac{1}{\sqrt{\sigma_2}} \sum_{n=1}^{\infty} \frac{1}{n} \frac{\partial^n \bar{R}}{\partial z^n} \Big|_{z=0} \rightarrow \text{finite}. \tag{3.48}$$

Now, we will have multiple images of the source if the deflection angle is greater than  $2\pi$ . The angular radius of the Einstein ring, which is created due to the symmetric lensing of light rays coming from some distant source, can be calculated using the strong-field deflection angle formula given in (3.47) and the lens equation [146, (147)]. The observational signatures of the deflection angle will be discussed in the following section.

### 3.5 Non-equatorial lensing

So far, we have discussed equatorial lensing. In this section, we will briefly discuss about the non-equatorial lensing in Kerr–Newmann spacetime for small inclination. We assume that the inclination is  $\theta = \frac{\pi}{2} - \psi$ , with  $\psi$  being very small. To

conduct the analysis, we will closely follow the analysis presented in [79].

For the non-equatorial plane, the carter constant is  $\bar{K} \neq 0$ . Instead, for the small inward inclination angle, we can write down the constants in terms of the inclination angle  $\psi$  as follows:

$$L \approx \lambda, \tag{3.49}$$

$$\bar{K} \approx h^2 + (\lambda^2 - a^2)\phi^2, \text{ with } \phi \approx \frac{h}{\lambda}. \tag{3.50}$$

In principle, one can parameterize the light ray coming from infinity by three parameters  $(\phi, h, \lambda)$ . If there is no gravitational field, the projection of the photon line on the equatorial plane has a minimum distance from the origin which is  $\lambda$ . Now, for given  $\lambda$ , the vertical distance of the light ray from the plane is  $h$ , and finally,  $\phi$  is the inclination angle formed by the light ray with the equatorial plane.

Now, using the  $\theta$  and  $\phi$  geodesic equation in (3.3) and requiring  $\psi$  to be small, we will have

$$\frac{d\psi}{d\phi} = \omega(r(\phi)) \sqrt{\hat{\psi}^2 - \psi^2}, \text{ with } \hat{\psi} = \sqrt{\frac{h^2}{\lambda^2 - a^2} + \phi^2}. \tag{3.51}$$

Now, we are interested in computing the deflection angle. For that, we first write down the following equation:

$$\bar{\phi}_f = \int_0^{\phi_f} d\phi \omega(\phi), \tag{3.52}$$

where  $\phi_f$  is the total azimuthal shift. Then, the deflection angle can be written as follows:

$$\hat{\alpha} = -\pi + 2 \int_{r_0}^{\infty} dr \omega(r) \frac{d\phi}{dr} = \int_0^1 dz \omega(r(z)) \bar{R}(z, r_0) \bar{F}(z, r_0), \tag{3.53}$$

where

$$\omega(r) = \bar{\lambda} \frac{a^2 + r(r-2)}{r(2a + \lambda(r-2)) + Q^2(\lambda-a)}, \tag{3.54}$$

with  $\bar{\lambda} = \sqrt{\lambda^2 - a^2}$ . We can follow the same method as mentioned in Section 3.4 to extract the divergent part as well as the finite part of the deflection angle as the function  $\omega(r)$ . They are given by

$$\hat{\alpha} = -\hat{a} \log\left(\frac{\lambda}{\lambda_c} - 1\right) + \hat{b}, \tag{3.55}$$

where

$$\hat{a} = \frac{\omega(z=0, r_c) \bar{R}(z=0, r_c)}{2\sqrt{\sigma_{2c}}}, \tag{3.56}$$

$$\hat{b} = -\pi + \hat{b}_R + \hat{a} \log\left(\frac{4\sigma_{2c} \bar{C}_c}{\lambda_c \bar{A}_c (\bar{D}_c + 2\lambda_c \bar{A}_c)}\right), \tag{3.57}$$

and

$$\hat{b}_R = \int_0^1 dz [\omega(z, r_c) \bar{R}(z, r_c) \bar{F}(z, r_c) - \omega(z=0, r_c) \bar{R}(z=0, r_c) \bar{F}(z, r_c)]. \tag{3.58}$$

Our interest is to find the position of the caustics, where the magnification diverges, and is given in [79],  $\bar{y}_k = -\bar{b} + \bar{a}(\hat{b} - k\pi)$ . Here,  $k$  is a positive integer. We have one caustic for the direct photon and one for the retrograde photon for each value of  $k$ . We

will find the caustic point in the weak-field limit for  $k = 1$  and the strong-field limit for  $k \geq 1$ , which is the regime of interest to us. In the next section, we give the results for caustic points in a more generic setup, that is, for the black-bounce metric. By taking the limit,  $l = 0$ , one can reproduce the results for the Kerr–Newman case. Furthermore from Eq. 3.54, one can see  $\omega(r) = 1$  implying that for Schwarzschild metric, there is no such difference between the equatorial and non-equatorial case.

## 4 Lensing for Kerr–Newman black-bounce spacetime

Before proceeding further, we will discuss how to calculate the exact deflection angle for Kerr–Newman black-bounce spacetime [137] and then go to the observational signatures gradually. It is interesting to study because it has one more parameter (apart from mass, rotation, and charge) that regularizes the central singularity. One can reproduce the results for Schwarzschild, Kerr, and Kerr–Newman spacetimes by taking appropriate limits. We start by applying the general formalism of lensing in this special kind of axisymmetric non-singular spacetime. We will closely follow the notation of [120] throughout this section.

### 4.1 Brief review of Kerr–Newman black-bounce spacetime

We will begin with a brief discussion of the null geodesics in Kerr–Newman black-bounce spacetime. To perform that, we first write the corresponding metric in the Boyer–Lindquist coordinate [137].

$$ds^2 = g_{\mu\nu} dx^\mu dx^\nu = -\frac{\Delta}{\Sigma} (a \sin^2 \theta d\phi - dt)^2 + \frac{\sin^2 \theta}{\Sigma} ((r^2 + a^2 + l^2)d\phi - a dt)^2 + \Sigma \left( \frac{dr^2}{\Delta} + d\theta^2 \right), \tag{4.1}$$

where

$$\Sigma = r^2 + l^2 + a^2 \cos^2 \theta, \Delta(r) = (r^2 + a^2 + l^2) - 2m\sqrt{r^2 + l^2} + Q^2. \tag{4.2}$$

Here,  $m \geq 0$  is the ADM mass,  $Q$  is the black hole charge parameter, and  $a = \frac{l}{m}$  corresponds to the angular momentum per mass. The non-vanishing regularizing parameter  $l > 0$  accounts for the absence of the central singularity. Keeping in mind that the radial coordinate’s range in this instance is  $-\infty < r < \infty$ , in the  $Q = 0, l = 0$  limit, we recover the Kerr metric. The location of the event horizon can be determined by equating  $\Delta(r) = 0$ .

$$R_H = \sqrt{\left[ (m + \sqrt{m^2 - (a^2 + Q^2)})^2 - l^2 \right]}. \tag{4.3}$$

We also need to impose the reality condition. That gives

$$m^2 - (a^2 + Q^2) > 0 \quad \text{and} \quad m + \sqrt{m^2 - (a^2 + Q^2)} > l.$$

Following the procedure mentioned in Section 3, one can obtain the turning point and radius of the photon sphere.

### 4.2 Perturbative computation of the deflection angle: Analytical results

Following the analysis mentioned in Section 3.3, one can write down the integral form of the deflection angle which is given by

$$\hat{\alpha} = -\pi + 2 \int_0^{\frac{1}{\sqrt{r_0^2+l^2}}} \frac{1}{\sqrt{1-l^2u^2}} \left[ \frac{1 - (2mu - Q^2u^2)(1-\frac{a}{\lambda})}{1 - 2mu + (a^2 + Q^2)u^2} \right] \frac{1}{\sqrt{B(u)}} \tag{4.4}$$

The polynomial  $B(u)(1 - l^2u^2)$  in (4.4) has *degree six*. As a result, we cannot write this integral as an elliptic integral in its entirety. However, in order to make some analytical headway, we will make the following assumption:

$$l^2u^2 \ll 1. \tag{4.5}$$

Then, we can Taylor expand

$$\frac{1}{\sqrt{1-l^2u^2}} = 1 + \frac{l^2u^2}{2} + \mathcal{O}(l^4u^4).$$

Finally, keeping terms upto  $\mathcal{O}(l^4)$  in (4.4), we obtain

$$\hat{\alpha} = -\pi + 2 \int_0^{\frac{1}{\sqrt{r_0^2+l^2}}} du \left( 1 + \frac{l^2u^2}{2} \right) \left[ \frac{1 - (2mu - Q^2u^2)(1-\omega)}{1 - 2mu + (a^2 + Q^2)u^2} \right] \frac{1}{\sqrt{B(u)}} + \mathcal{O}(l^4) = \hat{\alpha}_{KN}|_{\sqrt{r_0^2+l^2}} + l^2 \xi(m, a, \lambda, Q) + \mathcal{O}(l^4), \tag{4.6}$$

where

$$\hat{\alpha}_{KN}|_{\sqrt{r_0^2+l^2}} = -\pi + 2 \int_0^{\frac{1}{\sqrt{r_0^2+l^2}}} du \left[ \frac{1 - (2mu - Q^2u^2)(1-\omega)}{1 - 2mu + (a^2 + Q^2)u^2} \right] \frac{1}{\sqrt{B(u)}}.$$

In the  $l = 0$  limit,  $\hat{\alpha}_{KN}$  reduces to the deflection angle for the Kerr–Newman black hole as mentioned in (3.16) and

$$\xi(m, a, \lambda, Q) = \int_0^{\frac{1}{\sqrt{r_0^2+l^2}}} u^2 \left[ \frac{1 - (2mu - Q^2u^2)(1-\omega)}{1 - 2mu + (a^2 + Q^2)u^2} \right] \frac{1}{\sqrt{B(u)}} du, \tag{4.7}$$

with  $\omega = \frac{a}{\lambda}$ . We now rewrite  $B(u)$  as

$$B(u) = -Q^2(1-w)^2(u-u_1)(u-u_2)(u-u_3)(u-u_4), \tag{4.8}$$

where the roots are defined as

$$u_1 = \frac{X_1 - 2m - X_2}{4m\sqrt{r_0^2 + l^2}}, \tag{4.9}$$

$$u_2 = \frac{1}{\sqrt{r_0^2 + l^2}}, \tag{4.10}$$

$$u_3 = \frac{X_1 - 2m + X_2}{4m\sqrt{r_0^2 + l^2}}, \tag{4.11}$$

$$u_4 = \frac{2m}{Q^2} - \frac{X_1}{2m\sqrt{r_0^2 + l^2}}. \tag{4.12}$$

Again, we apply the same strategy as sketched in Appendix A for the Kerr–Newman case. We choose the constants  $X_1$  and  $X_2$  in such a way so that we can write down the roots in the following order  $u_1 < u_2 < u_3 < u_4$ . Similar to the Kerr–Newman case,  $u_2, u_3, u_4$  turn out to be the positive roots, while  $u_1$  turns to be a negative root. To find out the roots, we need to substitute Eqs 4.9–4.12 into (4.8) and compare it with the coefficients of  $u^0, u^2, u^3, u^4$  in (3.14), and then, we will obtain [144]

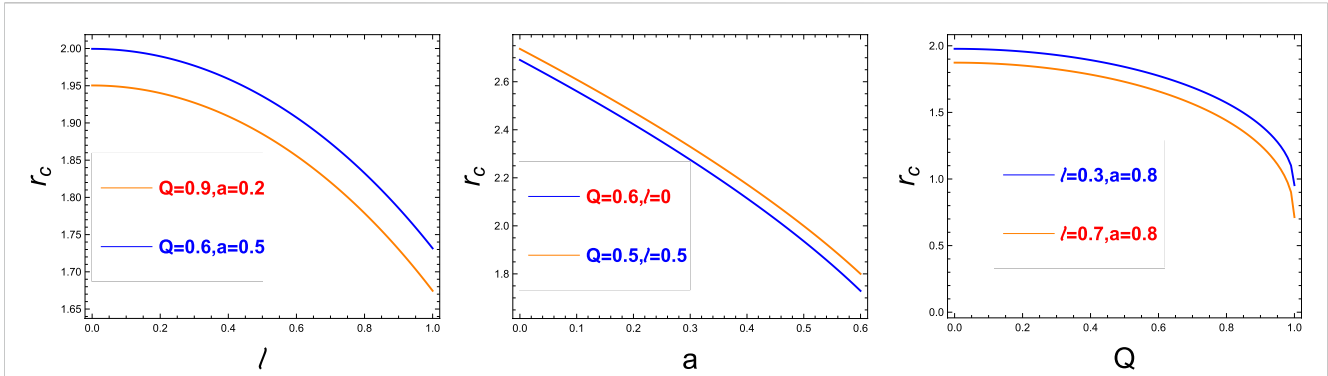


**FIGURE 1** Variation of radii of the photon sphere for charged, rotating Kerr–Newman black-bounce metrics for various values of  $(a, Q, l)$ . In the leftmost figure, we vary  $l$  keeping  $a$  and  $Q$  fixed. In the middle figure, we vary  $a$  keeping  $l$  and  $Q$ , and in the rightmost figure, we vary  $Q$  keeping  $a$  and  $l$  [120].

$$\begin{aligned}
 & Q^2 [X_2^2 - (X_1 - 2m)(X_1 + 6m) + 4X_1^2] \\
 &= 16m^2 \sqrt{r_0^2 + l^2} \left( X_1 - \sqrt{r_0^2 + l^2} \frac{1 + \omega}{1 - \omega} \right), \\
 & X_2^2 - (X_1 - 2m)^2 = \frac{8m(X_1 - 2m)(Q^2 X_1 - 4m^2 \sqrt{r_0^2 + l^2})}{Q^2(X_1 - 2m) - 4m^2 \sqrt{r_0^2 + l^2}}, \\
 & [X_2^2 - (X_1 - 2m)^2] \left( \frac{1}{8m(r_0^2 + l^2)^{\frac{3}{2}}} - \frac{Q^2 X_1}{32m^3(r_0^2 + l^2)^2} \right) \\
 &= \frac{1}{\lambda^2(1 - \omega)^2}. \tag{4.13}
 \end{aligned}$$

By exactly following the same procedure as in Section 3.3, one can write down the expression of deflection angle upto  $\mathcal{O}(l^2)$ , and the correction term is given by

$$\begin{aligned}
 \xi(m, a, \lambda, Q) &= \int_0^{u_2} du u^2 \left[ \frac{G_+}{u_+ - u} + \frac{G_-}{u_- - u} + \frac{G_{Q+} u}{u_+ - u} + \frac{G_{Q-} u}{u_- - u} \right] \\
 &\times \frac{1}{\sqrt{-Q^2(1 - \omega)^2(u - u_1)(u - u_2)(u - u_3)(u - u_4)}} \\
 &= G_+ g(u_+ \Delta F + [(u_1 - u_4) \Delta \Pi(\alpha^2) + u_4 \Delta F] \\
 &- u_+^2 \frac{1}{(u_+ - u_1)} \left[ \frac{u_1 - u_4}{u_+ - u_4} \Delta \Pi(\alpha_{\pm 3}^2) + \frac{u_+ - u_1}{u_+ - u_4} \Delta F \right]) \\
 &+ G_- g(u_- \Delta F + [(u_1 - u_4) \Delta \Pi(\alpha^2) + u_4 \Delta F] \\
 &- u_-^2 \frac{1}{(u_- - u_1)} \left[ \frac{u_1 - u_4}{u_- - u_4} \Delta \Pi(\alpha_{\pm 3}^2) + \frac{u_- - u_1}{u_- - u_4} \Delta F \right]) \\
 &+ G_{Q+} g \left[ \left( u_4^2 - 2u_+ u_4 + u_+^2 - \frac{u_+^3}{u_+ - u_4} \right) \Delta F \right. \\
 &+ \left. \left( u_+ (u_1 - u_4) - \frac{u_+^3 (u_1 - u_4)}{(u_+ - u_1)(u_+ - u_4)} \right) \Delta \Pi(\alpha_{\pm 3}^2) \right. \\
 &- \left. 2u_4 (u_1 - u_4) \chi_1(\alpha^2) - (u_1 - u_4)^2 \chi_2(\alpha^2) \right] \\
 &+ G_{Q-} g \left[ \left( u_4^2 - 2u_- u_4 + u_-^2 - \frac{u_-^3}{u_- - u_4} \right) \Delta F \right. \\
 &+ \left. \left( u_- (u_1 - u_4) - \frac{u_-^3 (u_1 - u_4)}{(u_- - u_1)(u_- - u_4)} \right) \Delta \Pi(\alpha_{\pm 3}^2) \right. \\
 &- \left. 2u_4 (u_1 - u_4) \chi_1(\alpha^2) - (u_1 - u_4)^2 \chi_2(\alpha^2) \right], \tag{4.14}
 \end{aligned}$$

where

$$\begin{aligned}
 \Delta F &= F(\psi_0, k) - F\left(\frac{\pi}{2}, k\right), \Delta \Pi(\alpha^2) = \Pi(\psi_0, \alpha^2, k) - \Pi\left(\frac{\pi}{2}, \alpha^2, k\right), \\
 \Delta \Pi(\alpha_{\pm 3}^2) &= \Pi(\psi_0, \alpha_{\pm 3}^2, k) - \Pi\left(\frac{\pi}{2}, \alpha_{\pm 3}^2, k\right) \tag{4.15}
 \end{aligned}$$

and  $\chi_1$  and  $\chi_2$  are given by

$$\begin{aligned}
 \chi_1(\alpha^2) &= \Pi\left(\frac{\pi}{2}, \alpha^2, k\right) - \Pi(\psi_0, \alpha^2, k), \\
 \chi_2(\alpha^2) &= \frac{1}{2(\alpha^2 - 1)(k^2 - \alpha^2)} \left[ \alpha^2 \left( E\left(\frac{\pi}{2}, k\right) - E(\psi_0, k) \right) \right. \\
 &+ (k^2 - \alpha^2) \left( F\left(\frac{\pi}{2}, k\right) - F(\psi_0, k) \right), \\
 &\left. (2\alpha^2 k^2 + 2\alpha^2 - \alpha^4 - 3k^2) \left( \Pi\left(\frac{\pi}{2}, \alpha^2, k\right) \right) - \Pi(\psi_0, \alpha^2, k) \right. \\
 &\left. - \frac{\alpha^4 \sin \psi_0 \sqrt{1 - \sin^2 \psi_0} \sqrt{1 - k^2 \sin^2 \psi_0}}{1 - \alpha^2 \sin^2 \psi_0} \right], \tag{4.16}
 \end{aligned}$$

and

$$\begin{aligned}
 g &= \frac{2}{\sqrt{Q^2(1 - \omega)^2(u_4 - u_2)(u_3 - u_1)}}, \alpha^2 = \frac{u_1 - u_2}{u_4 - u_2} < 0, \\
 \alpha_{\pm 3}^2 &= \alpha^2 \frac{u_{\pm} - u_4}{u_{\pm} - u_1}, k^2 = \frac{(u_4 - u_3)(u_2 - u_1)}{(u_4 - u_2)(u_3 - u_1)}, \\
 \psi_0 &= \arcsin \sqrt{\frac{(X_2 + 2m - X_1) \left[ 4m^2 \sqrt{r_0^2 + l^2} - Q^2(X_1 + 2m) \right]}{(X_2 + 6m - X_1) \left( 4m^2 \sqrt{r_0^2 + l^2} - Q^2 X_1 \right)}}. \tag{4.17}
 \end{aligned}$$

$\Pi(\psi_0, \alpha^2, k)$  and  $\Pi\left(\frac{\pi}{2}, \alpha^2, k\right)$  are the incomplete and complete elliptic integrals of the third kind, respectively. On the other hand,  $F(\psi_0, k)$  and  $F\left(\frac{\pi}{2}, k\right)$  are the incomplete and complete first-kind elliptic integrals, respectively. In addition, we have  $E(\psi_0, k)$  and  $E\left(\frac{\pi}{2}, k\right)$  in  $V_{1,2}$ , which are incomplete and complete elliptic integrals of the second kind, respectively. The computation details are given in [120]. So, similar to the Kerr–Newman case, we provide an analytical expression of the equatorial deflection angle for the Kerr–Newman black-bounce metric upto  $\mathcal{O}(l^2)$  in this section.

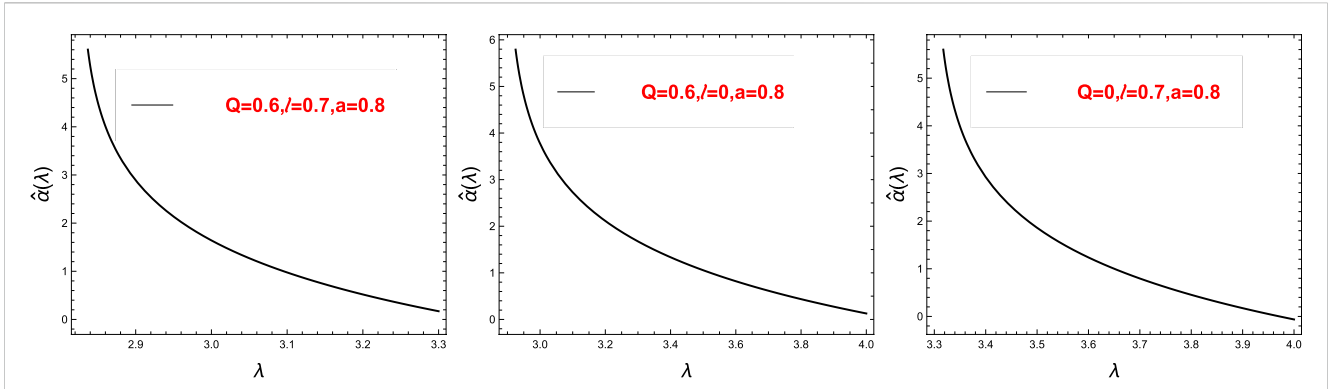


FIGURE 2 Variation of the deflection angle  $\hat{\alpha}$  with respect to the impact parameter  $\lambda$  for fixed values of  $Q, l, a$  [120].

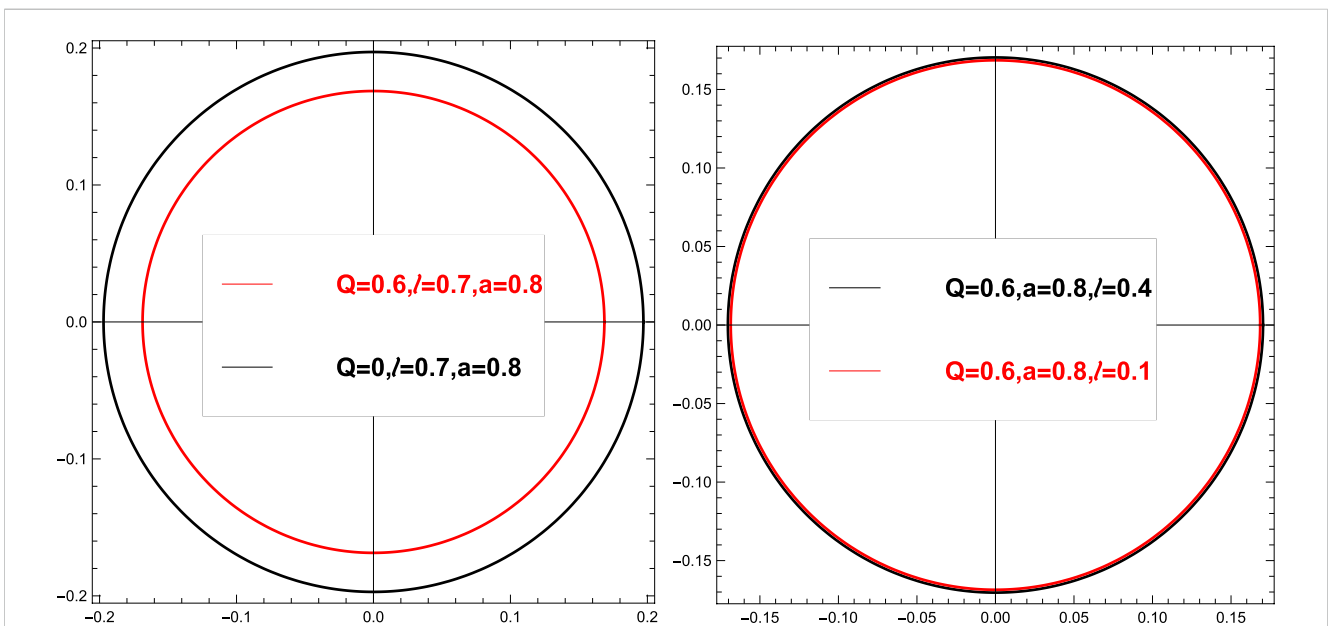


FIGURE 3 Polar plots showing the angular radius  $\theta_1$  for different  $Q, l, a$  values [120].

TABLE 1 Percentage change in the angular radius of the first Einstein ring for different values of charge  $Q$  for fixed  $a$  and  $l$ . Some of the numerical values presented here are reproduced from [120].

Angular separation		Percentage change	Values of charge	Fixed parameter	
$\theta_1^{(1)}(Q_2)$	$\theta_1^{(2)}(Q_1)$	$\Delta\theta = \frac{(\theta_1^{(2)} - \theta_1^{(1)})}{\theta_1^{(1)}} \times 100$	$(Q_1, Q_2)$	$l$	$a$
0.1686	0.1970	16.9013	(0, 0.6)	0.7	0.8
0.18548	0.21590	16.399	(0.6, 0.8)	0.4	0.5
0.22691	0.24236	6.8088	(0.45, 0.65)	0.4	0.5

### 4.3 Strong deflection analysis

Following the same analysis given in Section 3.4, we can find out the deflection angle of equatorial light rays in the strong deflection limit. We will summarize the steps and results as follows:

- First, we write down the deflection angle as follows:

$$\phi(r_0) = \int_0^1 \bar{R}(z_2, r_0) \bar{F}(z_2, r_0) dz_2, \tag{4.18}$$

with

$$\bar{R}(z_2, r_0) = \frac{2(1 - y_0)}{A'} \frac{\sqrt{BA_0}(\bar{D} + 2L\bar{A})}{\sqrt{4AC^2 + \bar{C}D^2}}, \tag{4.19}$$

**TABLE 2** Percentage change in the angular radius of the first Einstein ring for different values of the regularization parameter  $l$  for  $a = 0.8$  and  $Q = 0.6$ . Some of the numerical values presented here are reproduced from [120].

Angular separation		Percentage change	Values of the regularization parameter
$\theta_1^{(1)}(l_1)$	$\theta_1^{(2)}(l_2)$	$\Delta\theta = \frac{(\theta_1^{(2)} - \theta_1^{(1)})}{\theta_1^{(1)}} \times 100$	$(l_1, l_2)$
0.16856	0.1703	1.07059	(0.2, 0.4)
0.16756	0.16760	0.023872	(0.25, 0.75)
0.166678	0.166680	0.001199	(0.15, 0.25)

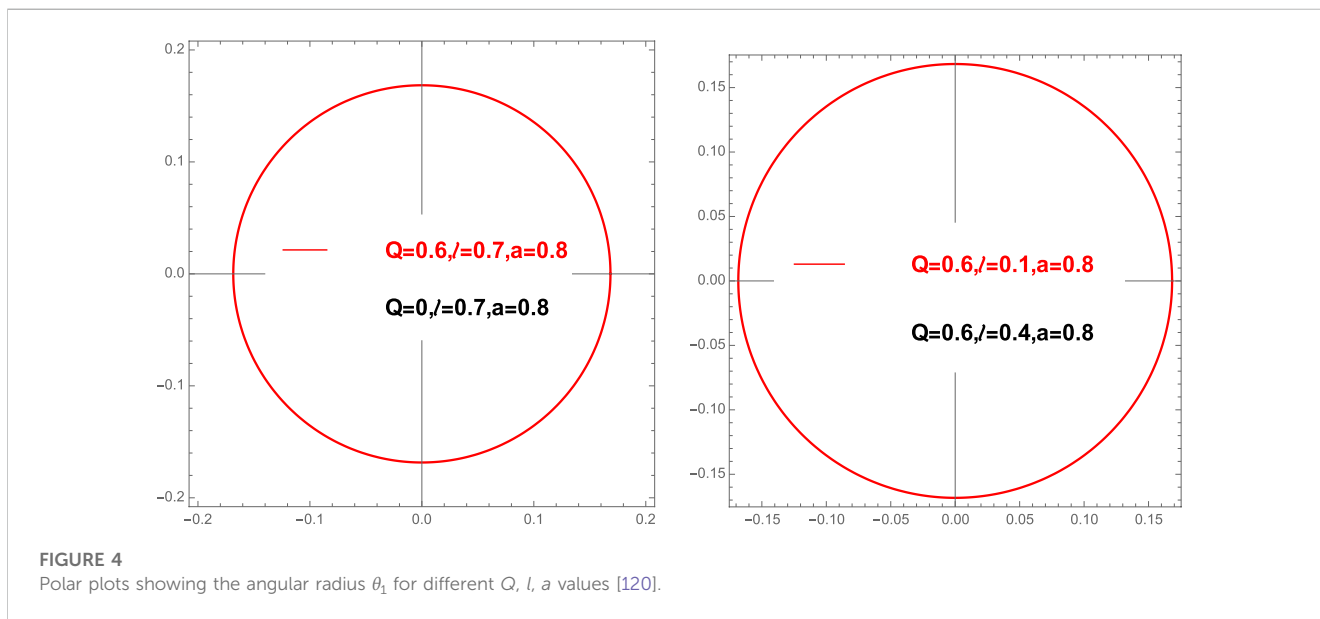


**FIGURE 4** Polar plots showing the angular radius  $\theta_1$  for different  $Q, l, a$  values [120].

$$\bar{F}(z_2, r_0) = \frac{1}{\sqrt{\frac{1}{C}(\bar{C}A_0 - \bar{A}C_0 + L(\bar{A}D_0 - \bar{D}A_0))}} = \frac{1}{\sqrt{H}} \quad (4.20)$$

$$\bar{H} = \frac{1}{C}(\bar{C}A_0 - \bar{A}C_0 + L(\bar{A}D_0 - \bar{D}A_0)). \quad (4.21)$$

The integral is potentially divergent at  $r_0 = r_c$ .

- Second, we separate the convergent and the divergent integral as

$$\phi(r_0) = \phi_{\bar{R}}(r_0) + \phi_F(r_0), \quad (4.22)$$

where

$$\begin{aligned} \phi_F(r_0) &= \int_0^1 \bar{R}(z_2 = 0, r_c) \bar{F}(z_2, r_0) dz_2. \rightarrow \text{the divergent part} \\ \phi_{\bar{R}}(r_0) &= \int_0^1 \bar{R}(z_2, r_0) \bar{F}(z_2, r_0) dz_2 \\ &\quad - \int_0^1 \bar{R}(z_2 = 0, r_c) \bar{F}(z_2, r_0) dz_2. \rightarrow \text{the finite part.} \end{aligned} \quad (4.23)$$

- Next, we find out the critical turning point  $r_c$  by solving the following equation:

$$\bar{A}_0 \bar{C}'_0 - \bar{A}'_0 \bar{C}_0 - L(\bar{A}_0 \bar{D}'_0 - \bar{A}'_0 \bar{D}_0)|_{r_0=r_c} = 0, \quad (4.24)$$

**TABLE 3** Angular position of the second caustic point for different values of  $Q$ . The first three entities are for direct photons, and the last three are for retrograde photons. Some of the numerical values presented here are reproduced from [120].

$(l, a)$	$Q$	$\bar{\sigma}_2$
(0.4, 0.5)	0.55	-6.28
(0.4, 0.5)	0.65	-4.98
(0.4, 0.5)	0.75	-0.137
(0.4, -0.5)	0.5	-5.69
(0.4, -0.5)	0.6	-5.84
(0.4, -0.5)	0.7	-5.90

which gives

$$\begin{aligned} &2a^2(Q^2 - m\sqrt{l^2 + r_c^2}) - 2a(Q^2 - m\sqrt{l^2 + r_c^2})\sqrt{a^2 - 2m\sqrt{l^2 + r_c^2} + l^2 + Q^2 + r_c^2 + l^4} \\ &l^2(-5m\sqrt{l^2 + r_c^2} + 6m^2 + 3Q^2 + 2r_c^2) - 7mQ^2\sqrt{l^2 + r_c^2} - 5mr_c^2\sqrt{l^2 + r_c^2} + 6m^2r_c^2 \\ &+ 2Q^4 + 3Q^2r_c^2 + r_c^4 = 0 \end{aligned} \quad (4.25)$$

We reproduce the results of [120] for the dependence of the critical turning point on different spacetime parameters ( $a, Q, l$ ) in Figure 1.

- At the end, we calculate the integrals in (4.23) at the limit  $r_0 \rightarrow r_c$  and we will find the logarithmic nature of the deflection

**TABLE 4** Angular position of the second caustic point for different values of  $l$ . The first three entities are for direct photons, and the last three are for retrograde photons. Some of the numerical values presented here are reproduced from [120].

$(Q, a)$	$l$	$\bar{\sigma}_2$
(0.5, 0.5)	0.45	-6.646
(0.5, 0.5)	0.55	-6.702
(0.5, 0.5)	0.65	-6.79
(0.5, -0.5)	0.7	-5.92
(0.5, -0.5)	0.8	-5.98
(0.5, -0.5)	1.0	-6.20

angle as shown in Figure 2. Again, we reproduce the result of [120] here.

### 4.4 Observational signature in the strong deflection limit

Now, we will discuss some observational consequences. The first step for this is to relate the deflection angle and the angular radius of the Einstein ring. This is performed by using a lens equation. In this paper, we will use the following lens equation [148]:

$$\beta = \theta - \frac{D_{LS}}{D_{OS}} \Delta\alpha_n, \tag{4.26}$$

where

$$D_{OS} = D_{OL} + D_{LS}.$$

Also,  $\beta$  is the angular separation between the source and the lens.  $D_{LS}$ ,  $D_{OS}$ ,  $D_{OL}$  are the distances between the lens to the source, the observer to the source, and the observer to the lens, respectively. Finally,

$$\Delta\alpha_n = \hat{\alpha}(\theta) - 2n\pi.$$

The angular separation between the lens and the  $n^{th}$  image can be written as follows:

$$\theta_n = \theta_n^0 + \Delta\theta_n,$$

where  $\theta_n^0$  is the angular separation between the  $n$  image and the lens when the extra deflection angle ( $\Delta\theta_n$ ) over  $2n\pi$  is negligible.

For the perfect alignment, that is, when  $\beta = 0$  and assuming  $\Delta\theta_n \ll \theta_n^0$ , the angular separation (angular radius) can be written as [79]

$$\theta_n^{Einstein} = \frac{\lambda_c}{D_{OL}} \left[ 1 + \exp\left(\frac{\bar{b}}{a} - \frac{2n\pi}{a}\right) \right]. \tag{4.27}$$

$n = 1$  corresponds to the outermost Einstein ring. Following [120], we plot some of these rings for different values of  $Q$ ,  $a$  and  $l$  in Figure 3.

From the leftmost plot in Figure 3, we can conclude that as the charge of the black hole  $Q$  increases (for fixed  $l$  and  $a$ ), the radii of the ring decrease. On the other hand, the effect of changing  $l$  (for fixed  $a$  and  $Q$ ) on

the ring radius is negligible. This is evident from the rightmost plot in Figure 3.

To make this observation more concrete, we carry out a detailed study, as shown in Tables 1, 2. Some of the values provided in (1) and (2) are reproduced from [120]. We have listed some values regarding the representative percentage change in the angular radius of the outermost Einstein rings with respect to  $Q$  (for fixed  $a$  and  $l$ ) and  $l$  (for fixed  $a$  and  $Q$ ) in Tables 1, 2, respectively. These values corroborate perfectly the conclusion drawn previously.

Before closing this section, a few comments regarding possible avenues to constraints on the spacetime parameters should be in order, utilizing observational data. One of the ways is to look into the ratio of mass to distance, the mass being the mass of the central object (e.g., Sagittarius A\*), which is around  $4.4 \times 10^6 M_\odot$  and its distance being 8.5 kpc, the ratio turns out to be around  $2.4734 \times 10^{-11}$ . One can use these data to provide the angular position of the relativistic images and the angular separation between the two Einstein rings. On the other hand, we can compute the angular separation of two successive Einstein rings from (4.27) for different values of  $n$ . Then, one can utilize it to build a parameter space for the spacetime parameters. Interested readers are referred to, for example, [107] for a more comprehensive discussion. In future detections, if one can better resolve the angular separation of various Einstein rings, we will get better constraints on the charge of the underlying black-bounce metric.

### 4.5 Results for non-equatorial lensing: Caustic points

In Section 3.5, we discussed about the non-equatorial lensing for the Kerr–Newman black hole. For this case also, the analysis would be the same. The only difference is that the scaling factor  $\omega(r)$  will be the function of the regularization parameter  $l$  apart from  $Q$  and  $a$ .

$$\omega(r) = \bar{\lambda} \frac{a^2 + \sqrt{r^2 + l^2} (\sqrt{r^2 + l^2} - 2)}{\sqrt{r^2 + l^2} (2a + \lambda (\sqrt{r^2 + l^2} - 2)) + Q^2 (\lambda - a)}, \tag{4.28}$$

with  $\bar{\lambda} = \sqrt{\lambda^2 - a^2}$ .

Next, we show how the angular radius of the first Einstein ring depends on  $Q$  and  $l$  in Figure 4 following [120]. It is evident from Figure 4 that the dependence of the angular radius on the charge parameter ( $Q$ ) of the black-bounce metric is significantly more than that on the regularization parameter ( $l$ ) similar to the case of equatorial lensing.

In Table 3, we investigate the variation of the second caustic point with respect to  $Q$  for fixed  $l$  and  $a$ .

Before closing this section, we further investigate the variation of the second caustic point with respect to  $l$  for fixed  $Q$  and  $a$ . It is demonstrated in Table 4. Comparing the values in Tables 3, 4, we can conclude that the change in caustic points for different  $Q$  and different  $l$  is not that robust [120].

## 5 Conclusion

As mentioned earlier, gravitational lensing studies provide an excellent tool to provide insight into the structure of spacetime itself. In light of these advantages, this review provides a brief tour of the analytic methods used to calculate observables which can be

measured. First, we review some facts about lensing in Schwarzschild geometry and observe the following points:

- The geodesics in this geometry are studied. As expected, owing to the symmetry of the spacetime itself, we have two constants of motion. Looking closely into the geodesic structures, we can find the location of the photon rings around them. Not only that, one can see that these photon rings located at  $3M$  are unstable, and one can seek out some non-trivial physics once you deviate infinitesimally from this range.
- After we have understood how geodesics behave in such a geometry, we can calculate quantities using the equations at hand. A comprehensive and self-explanatory calculation is provided which gives an estimate of the deflection angle in terms of the central massive object responsible for this deflection. The contribution of this central massive object in the formula is through the mass of the object. There is also a contribution from an  $r_{min}$  term in the denominator which indirectly also depends on the metric structure around the central massive object. We have also listed down some salient features related to the calculation in the bullet points in the following (Eq. 2.15).

After giving a brief overview of the time delay suffered by these geodesics and also going on to calculate the diameter of the Einstein ring in this setup, we move on to a more general spacetime having extra rotation parameters. As expected, all the aforementioned observables will have a non-trivial rotation parameter-dependent term. The calculations are all in the strong deflection limit and analytical. We also consider a more general class of proposed solutions called black-bounce spacetimes, where there is an extra parameter involved as a deviation of the already known solutions in GR. We list the salient features of our findings as follows:

- We presented a method of calculating the deflection angle analytically by performing a perturbation in  $l$ . The results are given in terms of elliptic integrals of various kinds. Also, we have restricted ourselves to the equatorial plane while performing this analysis. We observe that for non-zero  $l$ , the value of the deflection angle for a fixed impact parameter decreases. Our calculation provides a general methodology to compute deflection angles analytically in a perturbative series. In future, it will be interesting to go beyond this small  $l$  expansion. This will require a thorough numerical analysis.
- Next, we study the strong deflection limit of the equatorial deflection angle. This has direct observational implications because it provides information about the Einstein rings. We can conclude that the effect of the charge ( $Q$ ) on the size of the Einstein ring is much more pronounced than that of the regularization parameter ( $l$ ) for a fixed value of spin parameter  $a$ . We discovered that decreasing the charge ( $Q$ ) considerably increases the ring's size. This observation remained the same even when we computed the ring's radius for a small polar inclination.
- Furthermore, we extend our analysis for non-equatorial lensing. This enables us to compute the location of the caustic points. We again observed that the effect of the charge ( $Q$ ) on the position of caustic points is more pronounced than the regularization parameter ( $l$ ). Again, one can apply this method to different black hole spacetimes to obtain an exact analytical expression. The study of non-equatorial lensing presented in this review assumes a

small inclination angle. Again, it will be interesting to go beyond this regime.

Another interesting direction we could not include in this review is the analysis of the structure of the shadow. Interested readers are referred to this review [149] for more details about this topic. Analysis of the shadow structure complements the analysis of the Einstein ring, which is presented here. It provides further constraints on the different black hole parameters and various theories of gravity. Interested readers are again referred to [149] for relevant references for this.

The analysis of the deflection angle presented in this review can straightforwardly be repeated to other black-bounce spacetimes, for example, [150]. Finally, there are several other avenues which have been pursued recently in the context of strong deflection of light rays. One such thing is the study of multilevel images. This helps one to predict how much resolution is required to distinguish between different Einstein rings. One important aspect is also to study the two-point correlation function of intensity fluctuations on the photon ring, which result from the photon traveling through several orbits around the central object. This plays a significant role from the perspective of image analysis. This black-bounce metric might be subject to these studies along the lines of [151]. These investigations will support our efforts to communicate with plausible astrophysical settings.

## Author contributions

All authors listed have made a substantial, direct, and intellectual contribution to the work and approved it for publication.

## Funding

Research of AC was supported by the Prime Minister's Research Fellowship (PMRF-192002-1174) of Government of India. AB was supported by the Mathematical Research Impact Centric Support Grant (MTR/2021/000490) by the Department of Science and Technology Science and Engineering Research Board (India) and the Relevant Research Project grant (202011BRE03RP06633-BRNS) by the Board of Research in Nuclear Sciences (BRNS), Department of Atomic Energy (DAE), India.

## Conflict of interest

The authors declare that the research was conducted in the absence of any commercial or financial relationships that could be construed as a potential conflict of interest.

## Publisher's note

All claims expressed in this article are solely those of the authors and do not necessarily represent those of their affiliated organizations, or those of the publisher, the editors, and the reviewers. Any product that may be evaluated in this article, or claim that may be made by its manufacturer, is not guaranteed or endorsed by the publisher.

## References

- Dyson FW, Eddington AS, Davidson C. A determination of the deflection of light by the sun's gravitational field, from observations made at the total eclipse of may 29, 1919. *Phil Trans Roy Soc Lond A* (1920) 220:291–333.
- Carroll SM. *Lecture notes on general relativity* (1997). gr-qc/9712019.
- Jackiw R, Pi S-Y. Chern-Simons modification of general relativity. *Phys Rev D* (2003) 68:104012. doi:10.1103/physrevd.68.104012
- Kanti P, Mavromatos NE, Rizos J, Tamvakis K, Winstanley E. Dilatonic black holes in higher curvature string gravity. *Phys Rev D* (1996) 54:5049–58. [hep-th/9511071]. doi:10.1103/physrevd.54.5049
- Horndeski GW. Second-order scalar-tensor field equations in a four-dimensional space. *Int J Theor Phys* (1974) 10:363–84. doi:10.1007/bf01807638
- Eling C, Jacobson T, Mattingly D. Einstein-Aether theory. In: *Deserfest: A celebration of the life and works of stanley deser* (2004). p. 163–79. doi:10.1007/978-1-4010001.
- Moffat JW. Black holes in modified gravity (MOG). *Eur Phys J C* (2015) 75(4):175. [1412.5424]. doi:10.1140/epjc/s10052-015-3405-x
- Gao X. Unifying framework for scalar-tensor theories of gravity. *Phys Rev D* (2014) 90:081501. [1406.0822]. doi:10.1103/physrevd.90.081501
- Gao X, Yamaguchi M, Yoshida D. Higher derivative scalar-tensor theory through a non-dynamical scalar field. *JCAP* (2019) 03:006. [1810.07434]. doi:10.1088/1475-7516/2019/03/006
- Gross DJ, Witten E. Superstring modifications of Einstein's equations. *Nucl Phys B* (1986) 277:1–10. doi:10.1016/0550-3213(86)90429-3
- Gross DJ, Sloan JH. The quartic effective action for the heterotic string. *Nucl Phys B* (1987) 291:41–89. doi:10.1016/0550-3213(87)90465-2
- de Roo M, Suelmann H, Wiedemann A. The Supersymmetric effective action of the heterotic string in ten-dimensions. *Nucl Phys B* (1993) 405:326–66. [hep-th/9210099]. doi:10.1016/0550-3213(93)90550-9
- Lovelock D. The Einstein tensor and its generalizations. *J Math Phys* (1971) 12:498–501. doi:10.1063/1.1665613
- Lovelock D. The four-dimensionality of space and the einstein tensor. *J Math Phys* (1972) 13:874–6. doi:10.1063/1.1666069
- Lodge OJ. Gravitation and light. *Nature* (1919) 104:354. doi:10.1038/104354a0
- Chwolson O. *Traité de Physique, 5 vols.* Paris: Hermann (1906–1919).
- Chwolson O, Chwolson O. *Astr Nach* (1924) 221:329–30.
- Hewitt JN, Turner EL, Schneider DP, Burke BF, Langston GI, Lawrence CR. Unusual radio source MG1131+0456: A possible einstein ring. *Nature* (1988) 333:537–40. doi:10.1038/333537a0
- Hewitt JN, Turner EL, Lawrence CR, Schneider DP, Brody JP. A gravitational lens candidate with an unusually red optical counterpart. *Astron J* (1992) 104:968. doi:10.1086/116290
- Hewitt JN, Chen GH, Messier MD. Variability in the einstein ring gravitational lens MG 1131+0456. *Astron J* (1995) 109:1956. doi:10.1086/117421
- Hammer F, Le Fevre O, Angonin MC, Meylan G, Smette A, Surdej J, et al. 1131+0456: Discovery of the optical einstein ring with the NTT. *Astron Astrophys* 250 (1991) L5.
- James Webb Space Telescope Goddard Space Flight Center. *James Webb space telescope goddard space flight center* (2022). Available from: <https://webb.nasa.gov/>.
- Schneider P, Ehlers J, Falco EE. *Gravitational lenses* (1992).
- Perlick V. *Gravitational lensing from a spacetime perspective* (2010). 1010.3416.
- Wambsgans J. Gravitational lensing in astronomy. *Living Rev Relativity* (1998) 1:12. [astro-ph/9812021]. doi:10.12942/lrr-1998-12
- Event Horizon Telescope Collaboration, Akiyama K, Alberdi A, Alef W, Asada K, Azulay R, Baczko A-K, et al. First M87 event horizon telescope results. I. The shadow of the supermassive black hole. *Astrophys J Lett* (2019) 875:L1. [1906.11238].
- Event Horizon Telescope Collaboration, Akiyama K, Alberdi A, Alef W, Asada K, Azulay R, Baczko A-K, et al. First M87 event horizon telescope results. II. Array and instrumentation. *Astrophys J Lett* (2019) 875(1):L2. [1906.11239].
- Event Horizon Telescope Collaboration, Akiyama K, Alberdi A, Alef W, Asada K, Azulay R, Baczko A-K, et al. First M87 event horizon telescope results. III. Data processing and calibration. *Astrophys J Lett* (2019) 875(1):L3. [1906.11240].
- Event Horizon Telescope Collaboration, Akiyama K, Alberdi A, Alef W, Asada K, Azulay R, Baczko A-K, et al. First M87 event horizon telescope results. IV. Imaging the central supermassive black hole. *Astrophys J Lett* (2019) 875(1):L4. [1906.11241].
- Event Horizon Telescope Collaboration, Akiyama K, Alberdi A, Alef W, Asada K, Azulay R, Baczko A-K, et al. First M87 event horizon telescope results. V. Physical origin of the asymmetric ring. *Astrophys J Lett* (2019) 875(1):L5. [1906.11242].
- Event Horizon Telescope Collaboration, Akiyama K, Alberdi A, Alef W, Asada K, Azulay R, Baczko A-K, et al. First M87 event horizon telescope results. VI. The shadow and mass of the central black hole. *Astrophys J Lett* (2019) 875(1):L6. [1906.11243].
- Event Horizon Telescope Collaboration, Akiyama K, Alberdi A, Alef W, Algaba JC, Anantua R, Asada K, et al. First Sagittarius A\* event horizon telescope results. I. The shadow of the supermassive black hole in the center of the milky way. *Astrophys J Lett* (2022) 930(2):L12.
- Event Horizon Telescope Collaboration, Akiyama K, Alberdi A, Alef W, Algaba JC, Anantua R, Asada K, et al. First Sagittarius A\* event horizon telescope results. II. EHT and multiwavelength observations, data processing, and calibration. *Astrophys J Lett* (2022) 930(2):L13.
- Event Horizon Telescope Collaboration, Akiyama K, Alberdi A, Alef W, Algaba JC, Anantua R, Asada K, et al. First Sagittarius A\* event horizon telescope results. III. Imaging of the galactic center supermassive black hole. *Astrophys J Lett* (2022) 930(2):L14.
- Event Horizon Telescope Collaboration, Akiyama K, Alberdi A, Alef W, Algaba JC, Anantua R, Asada K, et al. First Sagittarius A\* event horizon telescope results. IV. Variability, morphology, and black hole mass. *Astrophys J Lett* (2022) 930(2):L15.
- Event Horizon Telescope Collaboration, Akiyama K, Alberdi A, Alef W, Algaba JC, Anantua R, Asada K, et al. First Sagittarius A\* event horizon telescope results. V. Testing astrophysical models of the galactic center black hole. *Astrophys J Lett* (2022) 930(2):L16.
- Event Horizon Telescope Collaboration, Akiyama K, Alberdi A, Alef W, Algaba JC, Anantua R, Asada K, et al. First Sagittarius A\* event horizon telescope results. VI. Testing the black hole metric. *Astrophys J Lett* (2022) 930(2):L17.
- Event Horizon Telescope Collaboration, Kocherlakota P, Rezzolla L, Falcke H, Fromm MC, Kramer M, Mizuno Y, et al. Constraints on black-hole charges with the 2017 EHT observations of M87\*. *Phys Rev D* (2021) 103(10):104047. [2105.09343].
- LIGO Scientific; Virgo Collaboration, Abbott BP, Abbott R, Abbott TD, Abernathy MR, Acernese F, Ackley K, et al. Observation of gravitational waves from a binary black hole merger. *Phys Rev Lett* (2016) 116(6):061102. [1602.03837]. doi:10.1103/PhysRevLett.116.061102
- LIGO Scientific; Virgo Collaboration, Abbott BP, Abbott R, Abbott TD, Abernathy MR, Acernese F, Ackley K, et al. Properties of the binary black hole merger GW150914. *Phys Rev Lett* (2016) 116(24):241102. [1602.03840]. doi:10.1103/PhysRevLett.116.241102
- LIGO Scientific; Virgo Collaboration, Abbott BP, Abbott R, Abbott TD, Abernathy MR, Acernese F, Ackley K, et al. GW151226: Observation of gravitational waves from a 22-solar-mass binary black hole coalescence. *Phys Rev Lett* (2016) 116(24):241103. [1606.04855]. doi:10.1103/PhysRevLett.116.241103
- LIGO Scientific; VIRGO Collaboration, Abbott BP, Abbott R, Abbott TD, Acernese F, Ackley K, Adams C, et al. GW170104: Observation of a 50-solar-mass binary black hole coalescence at redshift 0.2. *Phys Rev Lett* 118 (2017), no. 22, 221101 [1706.01812], [Erratum: Phys.Rev.Lett. 121, 129901 (2018)].
- LIGO Scientific; KAGRA-VIRGO Collaboration, Abbott R, Abbott TD, Abraham S, Acernese F, Ackley K, Adams C, et al. Observation of gravitational waves from two neutron star–black hole coalescences. *Astrophys J Lett* (2021) 915(1):L5. [2106.15163].
- KAGRA Collaboration, Kokeyama K. Observing the universe from underground gravitational wave telescope KAGRA. In: *3rd world summit on exploring the dark side of the universe* (2020). p. 41–8.
- LIGO Scientific; Virgo Collaboration, Abbott BP, Abbott R, Abbott TD, Acernese F, Ackley K, Adams C, et al. Tests of general relativity with the binary black hole signals from the LIGO-virgo catalog GWTC-1. *Phys Rev D* (2019) 100(10):104036. [1903.04467].
- LIGO Scientific; VIRGOKAGRA Collaboration, Abbott R, Abe H, Acernese F, Ackley K, Adhikari N, Adhikari RX, et al. *Tests of general relativity with GWTC-3* (2021). 2112.06861.
- Psaltis D, Abbott R, Abe H, Acernese F, Ackley K, Adhikari N, et al. Testing general relativity with the event horizon telescope. *Gen Rel Grav* (2019) 51(10):137. [1806.09740]. doi:10.1007/s10714-019-2611-5
- Himwich E, Johnson MD, Lupsasca A, Strominger A. Universal polarimetric signatures of the black hole photon ring. *Phys Rev D* (2020) 101(8):084020. [2001.08750]. doi:10.1103/physrevd.101.084020
- Gralla SE. Can the EHT M87 results be used to test general relativity? *Phys Rev D* (2021) 103(2):024023. [2010.08557]. doi:10.1103/physrevd.103.024023
- Vagnozzi S, Roy R, Tsai YD, Visinelli L. *Horizon-scale tests of gravity theories and fundamental physics from the Event Horizon Telescope image of Sagittarius A\** (2022). 2205.07787.
- Völkel SH, Barausse E, Franchini N, Broderick AE. EHT tests of the strong-field regime of general relativity. *Class Quant Grav* (2021) 38(21):21LT01. [2011.06812]. doi:10.1088/1361-6382/ac27ed
- Bambi C, Freese K, Vagnozzi S, Visinelli L. Testing the rotational nature of the supermassive object M87\* from the circularity and size of its first image. *Phys Rev D* (2019) 100(4):044057. [1904.12983]. doi:10.1103/physrevd.100.044057

53. Vagnozzi S, Visinelli L. Hunting for extra dimensions in the shadow of M87\*. *Phys Rev D* (2019) 100(2):024020. [1905.12421]. doi:10.1103/physrevd.100.024020
54. Allahyari A, Khodadi M, Vagnozzi S, Mota DF. Magnetically charged black holes from non-linear electrodynamics and the Event Horizon Telescope. *JCAP* (2020) 02:003. [1912.08231]. doi:10.1088/1475-7516/2020/02/003
55. Khodadi M, Allahyari A, Vagnozzi S, Mota DF. Black holes with scalar hair in light of the Event Horizon Telescope. *JCAP* (2020) 09:026. [2005.05992]. doi:10.1088/1475-7516/2020/09/026
56. Cunha PVP, Herdeiro CAR, Radu E, Runarsson HF. Shadows of Kerr black holes with scalar hair. *Phys Rev Lett* (2015) 115(21):211102. [1509.00021]. doi:10.1103/physrevlett.115.211102
57. Wang M, Chen S, Jing J. Shadow casted by a Konoplya-Zhidenko rotating non-Kerr black hole. *JCAP* (2017) 10:051. [1707.09451]. doi:10.1088/1475-7516/2017/10/051
58. Younsi Z, Zhidenko A, Rezzolla L, Konoplya R, Mizuno Y. New method for shadow calculations: Application to parametrized axisymmetric black holes. *Phys Rev D* (2016) 94(8):084025. [1607.05767]. doi:10.1103/physrevd.94.084025
59. Bisnovaty-Kogan GS, Tsupko OY. Shadow of a black hole at cosmological distances. *Phys Rev D* (2018) 98(8):084020. [1805.03311]. doi:10.1103/physrevd.98.084020
60. Banerjee I, Chakraborty S, SenGupta S. Silhouette of M87\*: A new window to peek into the world of hidden dimensions. *Phys Rev D* (2020) 101(4):041301. [1909.09385]. doi:10.1103/physrevd.101.041301
61. Tsupko OY, Bisnovaty-Kogan GS. First analytical calculation of black hole shadow in McVittie metric. *Int J Mod Phys D* (2020) 29(09):2050062. [1912.07495]. doi:10.1142/s0218271820500625
62. Tsupko OY, Fan Z, Bisnovaty-Kogan GS. Black hole shadow as a standard ruler in cosmology. *Class Quant Grav* (2020) 37(6):065016. [1905.10509]. doi:10.1088/1361-6382/ab6f7d
63. Mishra AK, Chakraborty S, Sarkar S. Understanding photon sphere and black hole shadow in dynamically evolving spacetimes. *Phys Rev D* (2019) 99(10):104080. [1903.06376]. doi:10.1103/physrevd.99.104080
64. Vagnozzi S, Bambi C, Visinelli L. Concerns regarding the use of black hole shadows as standard rulers. *Class Quant Grav* (2020) 37(8):087001. [2001.02986]. doi:10.1088/1361-6382/ab7965
65. Li P-C, Guo M, Chen B. Shadow of a spinning black hole in an expanding universe. *Phys Rev D* (2020) 101(8):084041. [2001.04231]. doi:10.1103/physrevd.101.084041
66. Perlick V, Tsupko OY. Light propagation in a plasma on Kerr spacetime: Separation of the Hamilton-Jacobi equation and calculation of the shadow. *Phys Rev D* (2017) 95(10):104003. [1702.08768]. doi:10.1103/physrevd.95.104003
67. Wei SW, Liu YX, Mann RB. Intrinsic curvature and topology of shadows in Kerr spacetime. *Phys Rev D* (2019) 99(4):041303. [1811.00047]. doi:10.1103/physrevd.99.041303
68. Chowdhuri A, Bhattacharyya A. Shadow analysis for rotating black holes in the presence of plasma for an expanding universe. *Phys Rev D* (2021) 104(6):064039. [2012.12914]. doi:10.1103/physrevd.104.064039
69. Papnoi U, Atamurotov F, Ghosh SG, Ahmedov B. Shadow of five-dimensional rotating Myers-Perry black hole. *Phys Rev D* (2014) 90(2):024073. [1407.0834]. doi:10.1103/physrevd.90.024073
70. Lin F-L, Patel A, Pu HY. *Black hole shadow with soft hair* (2022). 2202.13559.
71. Chandrasekhar S. *The mathematical theory of black holes. Oxford classic texts in the physical sciences*. Oxford: Oxford Univ. Press (2002).
72. Adler SL, Virbhadra KS. *Cosmological constant corrections to the photon sphere and black hole shadow radii* (2022). 2205.04628.
73. Virbhadra KS. *Compactness of supermassive dark objects at galactic centers* (2022). 2204.01792.
74. Roy R, Vagnozzi S, Visinelli L. Superradiance evolution of black hole shadows revisited. *Phys Rev D* (2022) 105(8):083002. [2112.06932]. doi:10.1103/physrevd.105.083002
75. Chen Y, Roy R, Vagnozzi S, Visinelli L. *Superradiant evolution of the shadow and photon ring of Sgr A\** (2022). 2205.06238.
76. Bozza V. Gravitational lensing in the strong field limit. *Phys Rev D* (2002) 66:103001. [gr-qc/0208075]. doi:10.1103/physrevd.66.103001
77. Virbhadra KS, Ellis GFR. Schwarzschild black hole lensing. *Phys Rev D* (2000) 62:084003. [astro-ph/9904193]. doi:10.1103/physrevd.62.084003
78. Frittelli S, Kling TP, Newman ET. Space-time perspective of Schwarzschild lensing. *Phys Rev D* (2000) 61:064021. [gr-qc/0001037]. doi:10.1103/physrevd.61.064021
79. Bozza V. Quasiequatorial gravitational lensing by spinning black holes in the strong field limit. *Phys Rev D* (2003) 67:103006. [gr-qc/0210109]. doi:10.1103/physrevd.67.103006
80. Bozza V. Comparison of approximate gravitational lens equations and a proposal for an improved new one. *Phys Rev D* (2008) 78:103005. [0807.3872]. doi:10.1103/physrevd.78.103005
81. Einstein A. Lens-like action of a star by the deviation of light in the gravitational field. *Science* (1936) 84:506-7. doi:10.1126/science.84.2188.506
82. Eiroa EF, Sendra CM. Gravitational lensing by a regular black hole. *Class Quant Grav* (2011) 28:085008. [1011.2455]. doi:10.1088/0264-9381/28/8/085008
83. Bin-Nun AY. Strong gravitational lensing by Sgr A\*. *Quant Grav* (2011) 28:114003. [1011.5848]. doi:10.1088/0264-9381/28/11/114003
84. Amarilla L, Eiroa EF, Giribet G. Null geodesics and shadow of a rotating black hole in extended Chern-Simons modified gravity. *Phys Rev D* (2010) 81:124045. [1005.0607]. doi:10.1103/physrevd.81.124045
85. Stefanov IZ, Yazadjiev SS, Gylchev GG. Connection between black-hole quasinormal modes and lensing in the strong deflection limit. *Phys Rev Lett* (2010) 104:251103. [1003.1609]. doi:10.1103/physrevlett.104.251103
86. Wei S-W, Liu YX, Fu CE, Yang K. Strong field limit analysis of gravitational lensing in Kerr-Taub-NUT spacetime. *JCAP* (2012) 10:053. [1104.0776]. doi:10.1088/1475-7516/2012/10/053
87. Chen S, Liu Y, Jing J. Strong gravitational lensing in a squashed Kaluza-Klein Gödel black hole. *Phys Rev D* (2011) 83:124019. [1102.0086]. doi:10.1103/physrevd.83.124019
88. Gylchev GN, Stefanov IZ. Gravitational lensing by phantom black holes. *Phys Rev D* (2013) 87(6):063005. [1211.3458]. doi:10.1103/physrevd.87.063005
89. Tsukamoto N, Harada T, Yajima K. Can we distinguish between black holes and wormholes by their Einstein ring systems? *Phys Rev D* (2012) 86:104062. [1207.0047]. doi:10.1103/physrevd.86.104062
90. Sahu S, Patil M, Narasimha D, Joshi PS. Can strong gravitational lensing distinguish naked singularities from black holes? *Phys Rev D* (2012) 86:063010. [1206.3077]. doi:10.1103/physrevd.86.063010
91. Chen S, Jing J. Strong gravitational lensing by a rotating non-Kerr compact object. *Phys Rev D* (2012) 85:124029. [1204.2468]. doi:10.1103/physrevd.85.124029
92. Wei SW, Liu YX. Observing the shadow of Einstein-Maxwell-Dilaton-Axion black hole. *JCAP* (2013) 11:063. [1311.4251]. doi:10.1088/1475-7516/2013/11/063
93. Atamurotov F, Abdurjabbarov A, Ahmedov B. Shadow of rotating non-Kerr black hole. *Phys Rev D* (2013) 88(6):064004. doi:10.1103/physrevd.88.064004
94. Eiroa EF, Sendra CM. Regular phantom black hole gravitational lensing. *Phys Rev D* (2013) 88(10):103007. [1308.5959]. doi:10.1103/physrevd.88.103007
95. Wei SW, Yang K, Liu YX. Black hole solution and strong gravitational lensing in Eddington-inspired Born-Infeld gravity. *Eur Phys J C* (2015) 75:253. [1405.2178], [Erratum: Eur.Phys.J.C 75, 331 (2015)]. doi:10.1140/epjc/s10052-015-3469-7
96. Tsukamoto N, Kitamura T, Nakajima K, Asada H. Gravitational lensing in Tangherlini spacetime in the weak gravitational field and the strong gravitational field. *Phys Rev D* (2014) 90(6):064043. [1402.6823]. doi:10.1103/physrevd.90.064043
97. Liu X, Jia J, Yang N. Gravitational lensing of massive particles in Schwarzschild gravity. *Class Quant Grav* (2016) 33(17):175014. [1512.04037]. doi:10.1088/0264-9381/33/17/175014
98. Wei SW, Liu YX, Fu CE. Null geodesics and gravitational lensing in a nonsingular spacetime. *Adv High Energ Phys*. (2015) 2015:1-11. [1510.02560]. doi:10.1155/2015/454217
99. Sotani H, Miyamoto U. Strong gravitational lensing by an electrically charged black hole in Eddington-inspired Born-Infeld gravity. *Phys Rev D* (2015) 92(4):044052. [1508.03119]. doi:10.1103/physrevd.92.044052
100. Bisnovaty-Kogan GS, Tsupko OY. Gravitational lensing in plasmic medium. *Plasma Phys Rep* (2015) 41:562-81. [1507.08545]. doi:10.1134/s1063780x15070016
101. Sharif M, Iftikhar S. Strong gravitational lensing in non-commutative wormholes. *Astrophys Space Sci* (2015) 357(1):85. doi:10.1007/s10509-015-2231-9
102. Younas A, Hussain S, Jamil M, Bahamonde S. Strong gravitational lensing by kiselev black hole. *Phys Rev D* (2015) 92(8):084042. [1502.01676]. doi:10.1103/physrevd.92.084042
103. Chen S, Jing J. Strong gravitational lensing for the photons coupled to Weyl tensor in a Schwarzschild black hole spacetime. *JCAP* (2015) 10:020. [1502.01088]. doi:10.1088/1475-7516/2015/10/020
104. Schee J, Stuchlik Z, Ahmedov B, Abdurjabbarov A, Toshmatov B. Gravitational lensing by regular black holes surrounded by plasma. *Int J Mod Phys D* (2017) 26(5):1741011. doi:10.1142/s0218271817410115
105. Man J, Cheng H. Analytical discussion on strong gravitational lensing for a massive source with af(R)global monopole. *Phys Rev D* (2015) 92(2):024004. [1205.4857]. doi:10.1103/physrevd.92.024004
106. Tsukamoto N. Deflection angle in the strong deflection limit in a general asymptotically flat, static, spherically symmetric spacetime. *Phys Rev D* (2017) 95(6):064035. [1612.08251]. doi:10.1103/physrevd.95.064035
107. Wang S, Chen S, Jing J. Strong gravitational lensing by a Konoplya-Zhidenko rotating non-Kerr compact object. *JCAP* (2016) 11:020. [1609.00802]. doi:10.1088/1475-7516/2016/11/020

108. Tsukamoto N. Strong deflection limit analysis and gravitational lensing of an Ellis wormhole. *Phys Rev D* (2016) 94(12):124001. [1607.07022]. doi:10.1103/physrevd.94.124001
109. Zhao F, Tang J, He F. Gravitational lensing effects of a Reissner–Nordström–de Sitter black hole. *Phys Rev D* (2016) 93(12):123017. doi:10.1103/physrevd.93.123017
110. Aldi GF, Bozza V. Relativistic iron lines in accretion disks: The contribution of higher order images in the strong deflection limit. *JCAP* (2017) 02:033. [1607.05365]. doi:10.1088/1475-7516/2017/02/033
111. Lu X, Yang FW, Xie Y. Strong gravitational field time delay for photons coupled to Weyl tensor in a Schwarzschild black hole. *Eur Phys J C* (2016) 76(7):357. [1606.02932]. doi:10.1140/epjc/s10052-016-4218-2
112. Cavalcanti RT, da Silva AG, da Rocha R. Strong deflection limit lensing effects in the minimal geometric deformation and Casadio–Fabbri–Mazzacurati solutions. *Class Quant Grav* (2016) 33(21):215007. [1605.01271]. doi:10.1088/0264-9381/33/21/215007
113. Zhao S-S, Xie Y. Strong field gravitational lensing by a charged Galileon black hole. *JCAP* (2016) 07:007. [1603.00637]. doi:10.1088/1475-7516/2016/07/007
114. Shaikh R, Kar S. Gravitational lensing by scalar-tensor wormholes and the energy conditions. *Phys Rev D* (2017) 96(4):044037. [1705.11008]. doi:10.1103/physrevd.96.044037
115. Rahman M, Sen AA. Astrophysical signatures of black holes in generalized proca theories. *Phys Rev D* (2019) 99(2):024052. [1810.09200]. doi:10.1103/physrevd.99.024052
116. Virbhadrha KS. *Distortions of images of Schwarzschild lensing* (2022). 2204.01879.
117. Hsieh T, Lee DS, Lin CY. Strong gravitational lensing by Kerr and Kerr–Newman black holes. *Phys Rev D* (2021) 103(10):104063. [2101.09008]. doi:10.1103/physrevd.103.104063
118. Hsieh T, Lee DS, Lin CY. Gravitational time delay effects by Kerr and Kerr–Newman black holes in strong field limits. *Phys Rev D* (2021) 104(10):104013. [2108.05006]. doi:10.1103/physrevd.104.104013
119. Ederly A, Godin J. Second order Kerr deflection. *Gen Rel Grav* (2006) 38:1715–22. doi:10.1007/s10714-006-0347-5
120. Ghosh S, Bhattacharyya A. Analytical study of gravitational lensing in Kerr–Newman black-bounce spacetime. *JCAP* (2022) 11:006. [2206.09954]. doi:10.1088/1475-7516/2022/11/006
121. Balazs NL. Effect of a gravitational field, due to a rotating body, on the plane of polarization of an electromagnetic wave. *Phys Rev* (1958) 110:236–9. doi:10.1103/physrev.110.236
122. Plebanski J. Electromagnetic waves in gravitational fields. *Phys Rev* (1960) 118:1396–408. doi:10.1103/physrev.118.1396
123. Atkinson RD. Light delays near a relativistic star. *Astron J* (1969) 74:320. doi:10.1086/110813
124. de Felice F. On the gravitational field acting as an optical medium. *Gen Relativity Gravitation* (1971) 2:347–57. doi:10.1007/bf00758153
125. Mashhoon B. Scattering of electromagnetic radiation from a black hole. *Phys Rev D* (1973) 7:2807–14. doi:10.1103/physrevd.7.2807
126. Mashhoon B. Influence of gravitation on the propagation of electromagnetic radiation. *Phys Rev D* (1975) 11:2679–84. doi:10.1103/physrevd.11.2679
127. Fischbach E, Freeman BS. Second-order contribution to the gravitational deflection of light. *Phys Rev D* (1980) 22:2950–2. doi:10.1103/physrevd.22.2950
128. Sereno M. Gravitational lensing in metric theories of gravity. *Phys Rev D* (2003) 67:064007. doi:10.1103/physrevd.67.064007
129. Ye X-H, Lin Q. A Simple optical analysis of gravitational lensing. *J Mod Opt* (2008) 55:1119–26. [0704.3485]. doi:10.1080/09500340701618395
130. Sen AK. A more exact expression for the gravitational deflection of light, derived using material medium approach. *Astrophysics* (2010) 53:560–9. doi:10.1007/s10511-010-9148-3
131. Roy S, Sen AK. Trajectory of a light ray in Kerr field: A material medium approach. *Astrophys Space Sci* (2015) 360(1):23. [1408.3212]. doi:10.1007/s10509-015-2538-6
132. Chakraborty S, Sen AK. Deflection of light due to rotating mass – A comparison among the results of different approaches. *J Phys Conf Ser* (2014) 481:012008. doi:10.1088/1742-6596/481/1/012008
133. Chakraborty S, Sen AK. *Light deflection in Kerr field for off-equatorial source* (2015). 1504.03124.
134. Simpson A, Visser M. Black-bounce to traversable wormhole. *JCAP* (2019) 02:042. [1812.07114]. doi:10.1088/1475-7516/2019/02/042
135. Lobo FSN, Rodrigues ME, Silva MVDS, Simpson A, Visser M. Novel black-bounce spacetimes: Wormholes, regularity, energy conditions, and causal structure. *Phys Rev D* (2021) 103(8):084052. [2009.12057]. doi:10.1103/physrevd.103.084052
136. Mazza J, Franzin E, Liberati S. A novel family of rotating black hole mimickers. *JCAP* (2021) 04:082. [2102.01105]. doi:10.1088/1475-7516/2021/04/082
137. Franzin E, Liberati S, Mazza J, Simpson A, Visser M. Charged black-bounce spacetimes. *JCAP* (2021) 07:036. [2104.11376]. doi:10.1088/1475-7516/2021/07/036
138. Tsukamoto N. Gravitational lensing in the Simpson–Visser black-bounce spacetime in a strong deflection limit. *Phys Rev D* (2021) 103(2):024033. [2011.03932]. doi:10.1103/physrevd.103.024033
139. Nascimento JR, Petrov AY, Porfirio PJ, Soares AR. Gravitational lensing in black-bounce spacetimes. *Phys Rev D* (2020) 102(4):044021. [2005.13096]. doi:10.1103/physrevd.102.044021
140. Guerrero M, Olmo GJ, Rubiera-García D, Gómez DSC. Shadows and optical appearance of black bounces illuminated by a thin accretion disk. *JCAP* (2021) 08:036. [2105.15073]. doi:10.1088/1475-7516/2021/08/036
141. Islam SU, Kumar J, Ghosh SG. Strong gravitational lensing by rotating Simpson–Visser black holes. *JCAP* (2021) 10:013. [2104.00696]. doi:10.1088/1475-7516/2021/10/013
142. Will CM. *Gravity: Newtonian, post-Newtonian, and general relativistic* (2016). p. 9–72.
143. Iyer SV, Hansen EC. Light’s bending angle in the equatorial plane of a Kerr black hole. *Phys Rev D* (2009) 80:124023. [0907.5352]. doi:10.1103/physrevd.80.124023
144. Hsiao YW, Lee DS, Lin CY. Equatorial light bending around Kerr–Newman black holes. *Phys Rev D* (2020) 101(6):064070. [1910.04372]. doi:10.1103/physrevd.101.064070
145. Claudel CM, Virbhadrha KS, Ellis GFR. The Geometry of photon surfaces. *J Math Phys* (2001) 42:818–38. [gr-qc/0005050]. doi:10.1063/1.1308507
146. Müller T. Einstein rings as a tool for estimating distances and the mass of a Schwarzschild black hole. *Phys Rev D* (2008) 77:124042. doi:10.1103/physrevd.77.124042
147. Virbhadrha KS. Relativistic images of Schwarzschild black hole lensing. *Phys Rev D* (2009) 79:083004. [0810.2109]. doi:10.1103/physrevd.79.083004
148. Bozza V, Capozziello S, Iovane G, Scarpetta G. Strong field limit of black hole gravitational lensing. *Gen Rel Grav* (2001) 33:1535–48. [gr-qc/0102068]. doi:10.1023/a:1012292927358
149. Perlick V, Tsupko OY. Calculating black hole shadows: Review of analytical studies. *Phys Rept* (2022) 947:1–39. [2105.07101]. doi:10.1016/j.physrep.2021.10.004
150. Barrientos J, Cisterna A, Mora N, Viganò A. AdS–Taub–NUT spacetimes and exact black bounces with scalar hair. *Phys Rev D* (2022) 106(2):024038. [2202.06706]. doi:10.1103/physrevd.106.024038
151. Hadar S, Johnson MD, Lupsasca A, Wong GN. Photon ring autocorrelations. *Phys Rev D* (2021) 103(10):104038. [2010.03683]. doi:10.1103/physrevd.103.104038

## Appendix A: Details of the computation of the deflection angle for Kerr–Newman spacetime

Here, we give details of computing the integral mentioned in (3.16). First, we rewrite  $B(u)$  in the factorized form.

$$B(u) = -Q^2(1-\omega)^2(u-u_1)(u-u_2)(u-u_3)(u-u_4), \tag{A1}$$

where

$$u_1 = \frac{X_1 - 2m - X_2}{4mr_0}, \tag{A2}$$

$$u_2 = \frac{1}{r_0}, \tag{A3}$$

$$u_3 = \frac{X_1 - 2m + X_2}{4mr_0}, \tag{A4}$$

$$u_4 = \frac{2m}{Q^2} - \frac{X_1}{2mr_0}. \tag{A5}$$

Then, by choosing the constants  $X_1$  and  $X_2$ , we can write down the roots in the following order:  $u_1 < u_2 < u_3 < u_4$ . Here, the positive roots are  $u_2, u_3, u_4$ , while the negative root is  $u_1$ . Then, we substitute Eqs A2–A5 into (A1) and compare it with the coefficients of  $u_0, u_2, u_3, u_4$  in (3.14). This way, we can eventually extract the roots. That gives [144]

$$\begin{aligned} Q^2[X_2^2 - (X_1 - 2m)(X_1 + 6m) + 4X_1^2] &= 16m^2r_0\left(X_1 - r_0\frac{1+\omega}{1-\omega}\right), \\ X_2^2 - (X_1^2 - 2m)^2 &= \frac{8m(X_1 - 2m)(Q^2X_1 - 4m^2r_0)}{Q^2(X_1 - 2m) - 4m^2r_0}, \\ [X_2^2 - (X_1^2 - 2m)^2] &\left(\frac{1}{8mr_0^3} - \frac{Q^2X_1}{32m^3r_0^4}\right) = \frac{1}{\lambda^2(1-\omega)^2}. \end{aligned} \tag{A6}$$

Combining the first and second equation of (A6), we obtain the equation for  $X_1$ , which is given by

$$\begin{aligned} \frac{Q^2}{2m}X_1^3 - (Q^2 + 4mr_0)X_1^2 + \left(4m^2r_0 + 2mQ^2 + \frac{8m^3r_0^2}{Q^2} + \frac{2mr_0^2(1+\omega)}{(1-\omega)}\right)X_1 \\ = 4m^2Q^2 + \frac{4m^2r_0^2(1+\omega)}{(1-\omega)} + \frac{8m^2r_0^3(1+\omega)}{Q^2(1-\omega)}. \end{aligned} \tag{A7}$$

Eq. A7 can be exactly solved. The positive real root  $X_1(m, \omega, Q, r_0)$  turns out to be the one mentioned in (3.19) of Section 3.3.

From (3.20), one can easily check that when  $Q$  becomes zero,  $\delta$  becomes  $\pi$ . In that limit, (3.19) can be written as follows:

$$X_1(m, \omega, Q = 0, r_0) = r_0\frac{1+\omega}{1-\omega}. \tag{A8}$$

It then exactly reproduces the result for the Kerr black hole [143]. Furthermore, we can reproduce the result for the Reissner–Nordstrom black hole in the limit,  $a = 0$ , and the root of the equation (A7) then reduces to

$$X_1(m, Q, \omega = 1, r_c) = 2m\left(\frac{2mr_0}{Q^2} - 1\right)\Bigg|_{r_c}, \tag{A9}$$

where  $r_c$  is defined in (3.11), and the result (A9) matches with the result of [144].

Now, we try to factorize the remaining part of the integrand of (3.16). We obtain

$$\begin{aligned} \frac{1 - 2mu(1-\omega) + Q^2u^2(1-\omega)}{1 - 2mu + (a^2 + Q^2)u^2} &= \frac{G_+}{u_+ - u} + \frac{G_-}{u_- - u} + \frac{G_{Q+}u}{u_+ - u} \\ &+ \frac{G_{Q-}u}{u_- - u}, \end{aligned} \tag{A10}$$

where

$$u_{\pm} = \frac{m \pm \sqrt{m^2 - (a^2 + Q^2)}}{a^2 + Q^2}. \tag{A11}$$

$G_-, G_+, G_{Q+}, G_{Q-}$  are defined in (3.18) of Section 3.3. Also, we can easily see from (A11)  $u_{\pm}$  are positive.